"Estimation and Dispersion Modeling

of Aircraft Activity Emissions from Chania Airport"

Makridis Minas

Mechanical Engineer

Examination Committee:

Professor M. Lazaridis (Supervisor)

Associate Professor D. Kolokotsa

Assistant Professor P. Panagiotopoulou

Chania, 2018

Contents

Abstract

The objective of the present study is to evaluate the effect of civil aviation aircraft activity on local air quality during the year 2016, at the International Airport of Chania which is located at the North East of the city of Chania, of Crete Island in Greece. The aspects of the study include both the estimation of the quantities of the emissions and the modeling of their dispersion.

The examined pollutants species are carbon monoxide (CO), nitrogen oxides (NO_X), particulate matter with aerodynamic diameter 2,5μm or less (PM 2,5) and sulphur oxides (SO_X). Ultrafine PM is further examined, with respect to its number concentration. Moreover, carbon dioxide (CO_2) is also included due to its contribution to the climate change. The estimation of the emissions has been carried out according to the methodologies provided by ICAO technical documents, whereas the dispersion modeling has been achieved through the EPA's AERMOD which is considered a state of the art software system for this purpose. The modeled values are compared to the regulated values of the Directive 2008/50/EC. The study refers exclusively to the emissions from aircrafts' LTO cycles, since other airport emissions have not been taken into account.

The total number of LTO cycles performed by civil aviation aircrafts during the year 2016, was 10.324 and the respective annual fuel consumption reached 9.136t. Total amounts of the released pollutants of CO, NO_X, PM 2,5 and SO_X were estimated to be 66,4t, 136,95t, 2,976t and 9,136t, respectively. As regards the environmental interest for the climate change, annual CO_2 emissions reached 28.870t.

Dispersion models have showed that most of the examined pollutant species are not of great concern for the studied area, since their values have been much lower than the thresholds regulated by 2008/50/EC. However, the dispersion model of NO_X for the averaging period of 1 hour has revealed that emissions have been much higher than the regulated value of 200μg/m^3 with the maximum value of 887,25μg/m^3 been recorded inside the aircrafts' parking area at the North-West end of the airport. The exceedance suggested further examination of this pollutant, so models of one winter day and one summer day have been also developed.

Περίληψη

Ο αντικειμενικός σκοπός της παρούσας μελέτης είναι η αξιολόγηση της επίδρασης της δραστηριότητας των αεροσκαφών πολιτικής αεροπορίας στην ποιότητα αέρα τοπικής κλίμακας για το έτος 2016, στο Αεροδρόμιο των Χανίων που βρίσκεται βορειοδυτικά της πόλης των Χανίων της Νήσου Κρήτης στην Ελλάδα. Οι πτυχές της μελέτης περιλαμβάνουν την εκτίμηση των ποσοτήτων των εκπομπών και τη μοντελοποίηση της διασποράς τους.

Οι εξεταζόμενοι ρύποι είναι το μονοξείδιο του άνθρακα (CO), τα οξείδια του αζώτου (NO$_X$), η σωματιδιακή ύλη με κλάση σωματιδίων με αεροδυναμική διάμετρο 2,5μm ή μικρότερη (PM 2,5) καθώς και τα οξείδια του θείου (SO$_X$). Η υπέρλεπτη σωματιδιακή ύλη εξετάζεται ως προς την αριθμητική συγκέντρωση. Επιπλέον, περιλαμβάνεται το διοξείδιο του άνθρακα λόγω της συνεισφοράς του στην κλιματική αλλαγή. Η εκτίμηση των εκπομπών έχει πραγματοποιηθεί σύμφωνα με μεθοδολογίες που παρέχονται στα τεχνικά κείμενα του ICAO ενώ η μοντελοποίηση της διασποράς έχει επιτευχθεί με τη χρήση του AERMOD της Αμερικανικής Υπηρεσίας Περιβάλλοντος, το οποίο θεωρείται ένα καθιερωμένο λογισμικό για αυτόν τον σκοπό. Οι τιμές των μοντέλων συγκρίνονται με τα θεσμοθετημένα όρια της Οδηγίας 2008/50/EC. Η μελέτη αναφέρεται αποκλειστικά στις εκπομπές από τους κύκλους LTO των αεροσκαφών καθώς δεν έχουν συμπεριληφθεί λοιπές εκπομπές από το αεροδρόμιο.

Ο συνολικός αριθμός των πραγματοποιηθέντων κύκλων LTO από πολιτικά αεροσκάφη κατά το έτος 2016 ήταν 10.324 και η αντίστοιχη ετήσια κατανάλωση καυσίμων ανήλθε σε 9.136t. Οι συνολικές ποσότητες των εκλυθέντων ρύπων CO, NO$_X$, PM 2,5 και SO$_X$ εκτιμήθηκαν σε 66,4t, 136,95t, 2,976t και 9,136t, αντίστοιχα. Όσον αφορά το περιβαλλοντικό ενδιαφέρον για την κλιματική αλλαγή, οι εκπομπές CO$_2$ ανήλθαν σε 28.870t.

Τα μοντέλα διασποράς έδειξαν ότι οι περισσότεροι από τους εξεταζόμενους ρύπους δεν προκαλούν σημαντική ανησυχία για την υπό μελέτη περιοχή καθώς οι τιμές τους εμφανίζονται αρκετά χαμηλότερες των θεσμοθετημένων ορίων της Οδηγίας 2008/50/EC. Ωστόσο, το ωριαίο μοντέλο διασποράς των NO$_X$ φανερώνει ότι οι εκπομπές είναι αρκετά υψηλότερες από το ρυθμιζόμενο όριο των 200μg/m^3 με την ανώτερη τιμή να αγγίζει τα 887,25μg/m^3 και να καταγράφεται στην περιοχή στάθμευσης των αεροσκαφών στη βορειοδυτική πλευρά του αεροδρομίου. Αυτή η υπέρβαση συνέστησε την περεταίρω εξέταση του ρύπου και για αυτόν το λόγο αναπτύχθηκαν μοντέλα που αναφέρονται σε μία χειμερινή και μία θερινή ημέρα του έτους.

Λέξεις Κλειδιά: Αεροσκάφος, εκπομπές, LTO, διασπορά, AERMOD, Αεροδρόμιο Χανίων.

To my wife Georgia and my son Antonios

This page has been intentionally left blank.

1. Introduction

Emissions associated with aircraft activity are of major concern since they deteriorate the local air quality, and they contribute to the greenhouse effect and the global climate change. Airport local scale air quality is affected more directly due to the toxicity of the emissions. The pollutants from aircrafts engines exhausts include NO_X, SO_X, CO, unburnt hydrocarbons (HC's), particulate matter and soot [1], which threaten the human health in various ways depending on the individuals' exposure. The permitted levels of human exposure for every pollutant are regulated by the World Health Organization (WHO) [2] and the nations are obligated to comply. European Union has adopted the Directive 2008/50/EC [3] which regulates the threshold values for most of these pollutants.

Apart from the effects on human health due to direct exposure, these pollutants can produce secondary species with acute impacts. CO, NO_X and HC's are considered precursors of tropospheric ozone (O_3) [1]. NO_X and SO_X can capture moisture from the atmosphere forming the respective acids that end up on the ground via wet depositions, with catastrophic impacts to the soil and buildings due to their corrosive action [4]. In addition, NO_X and HC's co-participate in the reactions that lead to the formation of photochemical smog [5] which threatens both human health and flight safety by lowering the visibility. Moreover, it can be associated with transport phenomena reaching the nearby urban fabric and add to the already existing air pollution from other emission sources in the area.

Engines exhausts also release CO_2 and H_2O as they are the main products of the ideal combustion [1] and they also pose an environmental concern. In fact, aviation has been responsible for the 2% of the anthropogenic emissions of CO_2 in 1992 [6]. Moreover, in high altitudes the released H_2O, contained in the exhaust gases, leads to the formation of contrails and, consequently, of cirrus clouds. Eventually, cirrus clouds favor the local temperature increase as they absorb the electromagnetic radiation [6]. There is also an impact of contrails on flight safety since they can influence the aircraft trajectories [7].

Here we examine the environmental impact of aircrafts activity, induced by Chania Airport which is one of the three commercial airports at Crete Island, besides Heraklion Airport and Sitia Airport. Despite the prevailing fiscal recession in Greece, during 2016 the branch of aerial transportations met an increase of 5,7% compared to the traffic of 2015 [8], which is also reflected by the flight movements at Chania Airport.

Crete Island is considered one of the most popular tourist attractions. It is mentioned that the natural beauty of the island numbers 54 Natura 2000 sites and 23 of them are located at Chania region [9]. The increased traffic can be also attributed to the few transportation options of reaching the island which they are limited to air and marine media. Given that the

whole traffic load is shared by airports and naval ports, Chania Airport has been expected to contribute to a great extent to the local air pollution.

Chania Airport "Ioannis Daskalogiannis" (ICAO code LGSA) is located at Akrotiri peninsula 11,2km North East of the city of Chania and about 4,5km North of Souda Bay, in the West of Crete Island in Greece. The geographical coordinates of the Airport are 35°31'53" North, 24°09'04" East and the elevation is 149,4m [10]. These coordinates refer to the center of the main runway, which has also been considered the center point of the modeled area in this study. The use of Universal Transverse Mercator (UTM) coordinates has been mandatory during this study. Therefore, after the appropriate conversion, the UTM coordinates of the airport are 3935709 Northing and 241691 Easting, expressed in meters.

The orientation of the main runway is 110° - 290°, defining two respective alternative runway options for take-off and landing, i.e. "11" and "29", depending on the prevailing wind direction. The main runway has a nominal length of 3.348m and a nominal width of 45m. In parallel of the main runway there are two taxiways, one in the North East and one in the South West direction. Both taxiways have the same length as the main runway. Only the North East taxiway is used by civil aviation aircrafts [10]. The present study refers exclusively to designated civil aviation aircraft movements recorded during the year 2016. Private aircraft movements have not been included in this study.

The commercial aircraft activity of the airport has been studied according to the fundamental concept of the Landing and Take-Off (LTO) cycle which includes five discrete aircraft phases; approach below 3.000ft and landing, arrival (taxi-in) to the parking area, departure (taxi-out) from the parking area, take-off and climb out up to 3.000ft [11]. A schematic diagram of the LTO cycle is provided in Figure 1.1.
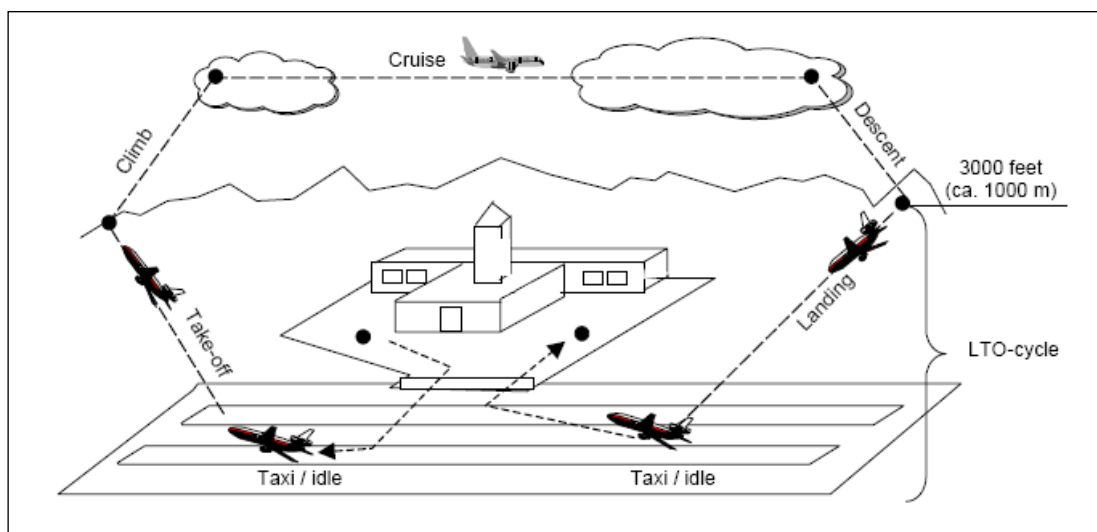

Figure 1.1: LTO modes performed at the airport territory [12].

Apart from taxi-in, taxi-out and take-off phases, which they are regarded as ground level operations within the airport site, the rest ones may cover a great deal of horizontal distance until the aircraft reduces its altitude from 3.000ft to ground level or reaches the altitude of 3.000ft after take-off. The respective horizontal distance of the height of 3.000ft has been determined by monitoring multiple B738 aircraft arrivals at the airport and departures from it, through a specialized web site [13]. The selection of this aircraft type has been made due to its common occurrence in several Greek airports.

The borders of the area of interest have been established by taking into account that there should be enough space for the emissions dispersion models to be presented. Moreover, the vicinity of the airport to several nearby settlements could provide a good overview of the environmental impact of the produced emissions. These facts suggested that the optimal expansion of the studied area should be 24km length by 16km width, which equals to 384km^2.

This page has been intentionally left blank.

2. State of the Art

Evaluation and modeling of the emissions produced by the aircraft activity can be achieved with the implementation of specialized measuring techniques which involve the usage of instruments dedicated for this purpose. Instead of using such experimental devices, the conduction of a complete environmental study about the air pollution induced by aircrafts can be accomplished without fieldwork but with the contribution of developed mathematical methodologies and software packages.

Several studies have been carried out according to the first option, i.e. with the establishment of measuring devices and monitoring a specific site for a specific time interval. Pollutant species of SO_2 are measured through the fluorescence technique [14], NO_X through the chemiluminescence detection (CLD) technique, both CO and CO_2 through the technique of non-dispersive infra-red (NDIR) and the unburnt hydrocarbons through the technique of flame ionization detection (FID) [15]. Moreover, other secondary emitted gases of the aircrafts exhausts can be measured through the differential optical absorption spectroscopy system (DOAS) [16]. Aethalometers are used to measure black carbon while particle sizers are used for the measurements related to particulate matter [15].

A study about aircraft emissions has been reported in 2011 and refers to an International Romanian Airport [17] with similar traffic characteristics to Chania Airport. This case study has evaluated the local air quality by means of point measurements of the pollutants (SO_2, NO_X, O_3, CO, and HC) with the mentioned measuring techniques. The sampling period was three 24 hour intervals of summer with increased traffic due to charter flight and the sampling site was set to the aircrafts' parking area where the maximum emission levels had been expected.

During two case studies about Los Angeles Airport that have been carried out aiming to evaluate the local air quality at the area of the airport, measuring instrumentation has been used, too. The environmental interest of these studies was based on the examination of particulate matter concentrations. One of the studies took place in September of 2005 and the sampling period was five continuous 24h intervals [18]. Two particle sizers were used to monitor the particles concentrations while the CO_2 readings were done via a Q-Track IAQ monitor, which incorporated NDIR technology.

The other study about the same airport was based on a sampling period of six randomly selected weekdays of May and July of the year 2016, in which measuring instrumentation was also used. Particle number and average particle size were evaluated with a diffusion size classifier and mass concentration has been measured with a dust track monitoring

device. Black carbon was measured with a microaetholometer and CO_2 with a NDIR analyzer [19].

Although measuring devices provide precise results for the studied location and the studied period, they fail to cover the whole examined site, since they are established at a certain point of the area. This position is usually where the maximum emissions are expected to occur. In order to acquire a satisfactory conclusion about the pollution dispersion at the examined area, researchers need to combine the measured data with mathematical and geospatial relationships to model the dispersion and to predict the emissions levels at locations with unavailability of data.

There has been a related case study about the aircraft emissions of NO_X, HC and CO at Marco Polo Airport, in Venice Italy [20]. During this study, two days of the year 2009 have been examined, one day of the summer and one day of the fall. This study has performed an air quality assessment by using both instrumentation and modeling media. The instrumentation included chemiluminescence, FID and IR photometry techniques for NO_X, HC and CO, respectively. The modeling section included diagnostic meteorological model (SWIFT), a turbulence processor (SURFPRO) and a 3D Langragian particle dispersion model [20].

Software packages which include functions for dispersion and geospatial predictions can mitigate the disadvantages of point measurements that provide results for a certain location. Moreover, the inclusion of the prevailing meteorological conditions can be achieved with the use of such software packages. Experiments are usually conducted during normal conditions and they are avoided during whether extremes, providing results with a great deal of uncertainty. On the other hand, the use of software packages incorporating routines for the inclusion of terrain topography, surface characteristics, land use and meteorological data, along with the intrinsic functions for emission dispersion and geospatial predictions, can provide a holistic approach during air pollution studies.

Studies about the emissions produced by aircrafts operating at commercial airports have been conducted using EPA's AERMOD because of its capability of incorporating the above attributes and combining various types of data for the pollution modeling. A study about a large commercial airport of Turkey (Atatürk International Airport) was reported in 2018 and refers to the year 2015 [21]. This study has examined the emissions dispersion of NO_X, CO and unburnt hydrocarbons over a period of one year, with the use of AERMOD. Compared to the reported annual traffic at this airport, the capacity of Chania Airport is about 3% of the capacity of Atatürk International Airport. Since the dispersion modeling has been carried out

with the use of AERMOD, the selection of AERMOD for the study of Chania Airport has provided fruitful comparisons.

A case study about Amerigo Vespucci Airport in Florence Italy has been conducted over the emissions of CO, NO_X and SO_X produced by aircraft activity during 2011 [22]. The traffic capacity of this airport is about two times greater than the capacity of Chania Airport which makes the two airports of a comparable interest. The emissions' modeling has been done with the usage of FAA's Emissions and Dispersion Modeling System (EDMS). This software includes a guided user interface capable of loading different options of emissions species, emissions sources, aircraft types and various types of vehicles related to the airport activities. The platform is connected to the dispersion processor of AERMOD [23].

It can be generally said that a good approach is the use of software and the cross-validation of the results with other ones which have used similar programs or they have been based on experimental measurements. Moreover, hybrid approaches of inserting the in situ measured values to a dedicated constructed model can provide satisfactory emissions dispersion modeling for the studied airport.

This page has been intentionally left blank.

3. Materials and Methods

The present study has been conducted without any measuring devices but with the exclusive use of computer software. EPA's AERMOD has been selected for this study because of its ability of incorporating a variety of different kinds of data of the examined environment. These data are meteorological, geographical, land use and emission related ones such source types, release heights and emission rates. The structure of AERMOD is consisted of several preprocessors, the main processor of AERMOD and the postprocessor of AERPLOT [24].

The locations of the emission sources, and the locations and the spacing of the emissions receptors are defined with the use of AERGRID preprocessor. AERMAP preprocessor creates the three dimensional map of the examined area by placing the output data of AERGRID over a required elevation file. AERSURFACE and AERMINUTE preprocessors process land use and wind data, respectively to provide input for the AERMET preprocessor. Finally, the main processor of AERMOD produces the model output. The postprocessor of AERPLOT produces the visual output of the model in the form of concentration contours [24]. Alternatively, the visualization can be achieved by inserting the output file of AERMOD to other software packages.

The main core processing functions of AERMOD are based on the Gaussian dispersion model which is a widely accepted mathematical model, due to its great operability when applied on computer programs. This model uses the Gaussian distribution to model the dispersion of non-reactant air pollutants produced by an elevated source, with the prediction of the steady state concentration at a specific point (x, y, z) and it is expressed by the Equation 2.1 [25].

$$C(x,y,z) = \frac{Q}{2\pi u \sigma_y \sigma_z} \exp\left(-\frac{1}{2}\frac{y^2}{\sigma_y^2}\right)\left\{\exp\left[-\frac{1}{2}\frac{(z-H)^2}{\sigma_z^2}\right] + \exp\left[-\frac{1}{2}\frac{(z+H)^2}{\sigma_z^2}\right]\right\} \quad (2.1)$$

where:
C : pollutant concentration at a steady state [$\mu g/m^3$];
Q : emission rate of the pollutant [$\mu g/s$];
u : wind speed at the source height, at direction x [m/s];
y : horizontal distance from the plume centerline;
z : vertical distance from the ground;
σ_y, σ_z : horizontal (y) and vertical (z) standard deviations of the distributions;
H : plume effective height (H=h+Δh, where h is the stack height and Δh the plume rise), [m];

The schematic diagram of the described model and its respective parameters is provided in Figure 3.1.
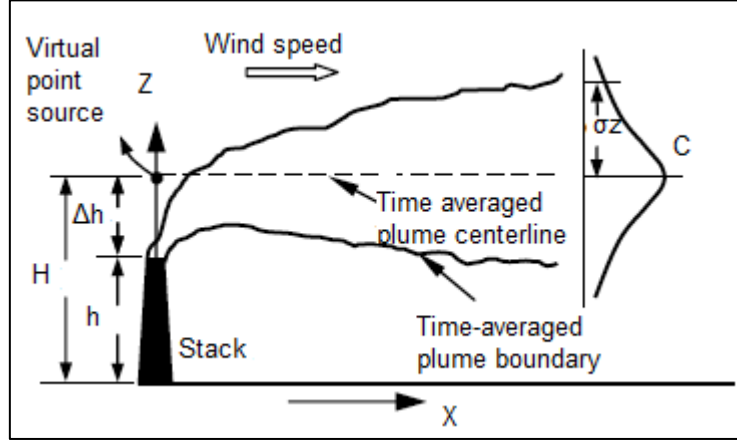

Figure 3.1: Gaussian distribution dispersion model (modified from [26]).

Equation 2.1 treats the plume dispersion as if it was developed in both directions of z-axis (-z, z) creating a "mirror" image of Figure 3.1. Since there cannot be any subterranean dispersion, the "mirror" image can be ignored by expelling the second last exponential of Equation 2.1 which, finally, takes the form of Equation 2.2 [25].

$$C(x,y,z) = \frac{Q}{2\pi u \sigma_y \sigma_z} \exp\left(-\frac{1}{2}\frac{y^2}{\sigma_y^2}\right) \exp\left[-\frac{1}{2}\frac{(z-H)^2}{\sigma_z^2}\right] \qquad (2.2)$$

For a receptor at the ground surface, or a source located at the ground (z=0), Equation 2.2 can be simplified to the form of Equation 2.3 [26].

$$C(x,y,0) = \frac{Q}{2\pi u \sigma_y \sigma_z} \exp\left(-\frac{y^2}{2\sigma_y^2} - \frac{H^2}{2\sigma_z^2}\right) \qquad (2.3)$$

One of the usual difficulties when evaluating the dispersion on a specific site is the lack of data at several locations. This obstacle can be outdistanced by performing geospatial predictions using the known values of neighboring positions. One of the most popular models for geospatial predictions is the model of kriging, which is described by the Equation 2.4 [27].

$$z^*(x_0) = \sum_{i=1}^{N} \lambda_i z(x_i) \qquad (2.4)$$

where:

x_0 : a target point for which a value is to be predicted;

$z(x_i)$: measured data at places x_i;

i : number of places;

λ_i : weights assigned to the measured data that can be determined with several methods;

3.1. Geographical Data

AERMAP preprocessor requires a suitable Digital Elevation Model (DEM) file in order to run. This file has been obtained from the United States Geological Survey (USGS) site [28] after the insertion of the coordinates of the four corners of the studied area. Since the length of the area was 24km and the width was 16km, the West and East longitudes were calculated by reducing and increasing the center point longitude by 12km, respectively. Similarly, the South and the North latitudes have been calculated by reducing and increasing the center point latitude by 8km, respectively.

The DEM file type has been selected from the available menu as a Shuttle Radar Topography Mission (SRTM) 1 Arc-Second Global. The acquired file was a geotiff image much bigger than the requested one. The coordinates of the acquired file was $[35^o, 36^o]$ North and $[24^o, 25^o]$ East, covering a large portion of west and central Crete Island. The position of both the requested and the acquired areas on the map is illustrated in red and black font respectively in Figure 3.2.
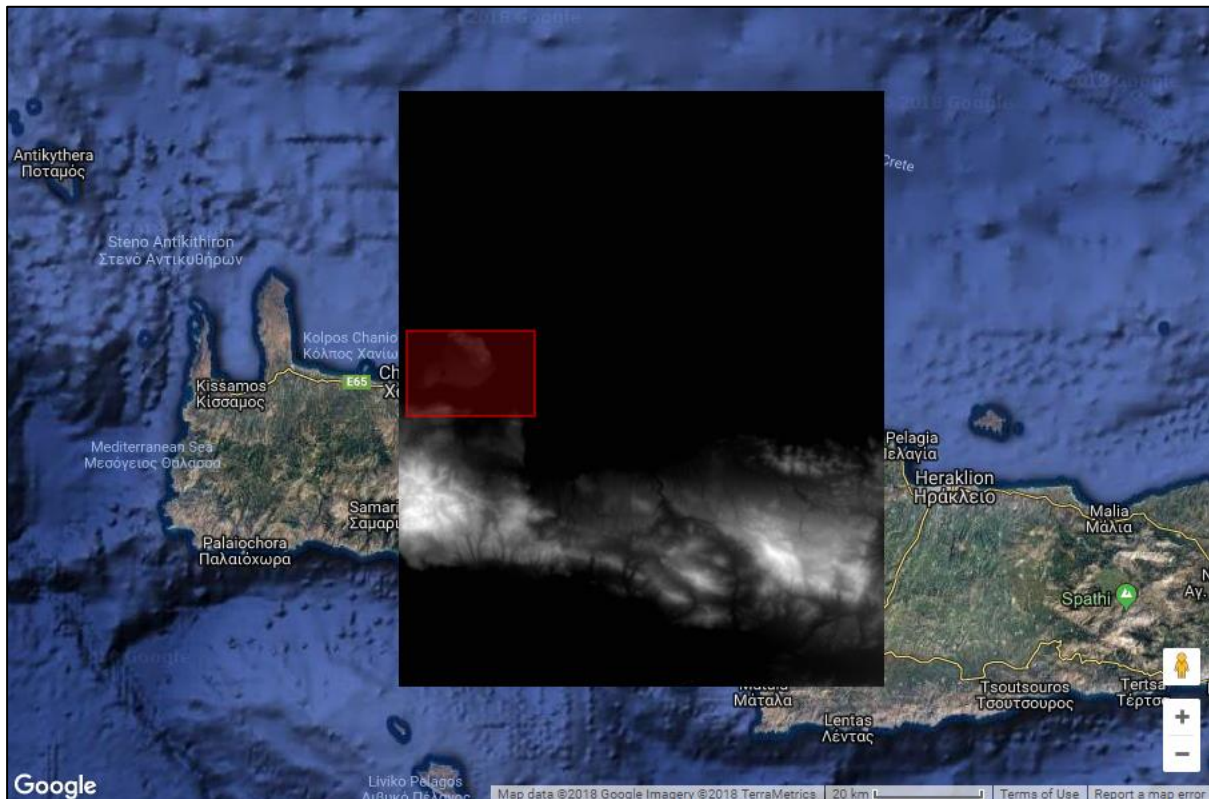

Figure 3.2: Requested (red) and acquired (black) areas (captured from [28]).

The acquired DEM file had to be inserted to Global Mapper software in order to view. After the insertion, the file has been cropped to the desired coordinates. Global Mapper revealed all the details about the studied area topography. The airport is located on a plane site of average elevation of 150m on Akrotiri peninsula. On the North of the airport there is a 10km

mountain range with a maximum elevation of 527m. The foothills of this formation create a plain with an elevation of 200m. There is also another mountainous formation in the very South of the studied area, with a maximum elevation of 609m. The soil type of the land area is basically rural.

Souda Bay is a natural port located in the middle of the area which forms a basin between these geological entities. The West coast of Akrotiri borders with Chania Gulf, whereas the North-East coast borders with Cretan Sea. The topography of the area is considered of great importance during the study of the emissions dispersion models. The discussed geographical characteristics are provided in Figure 3.3.
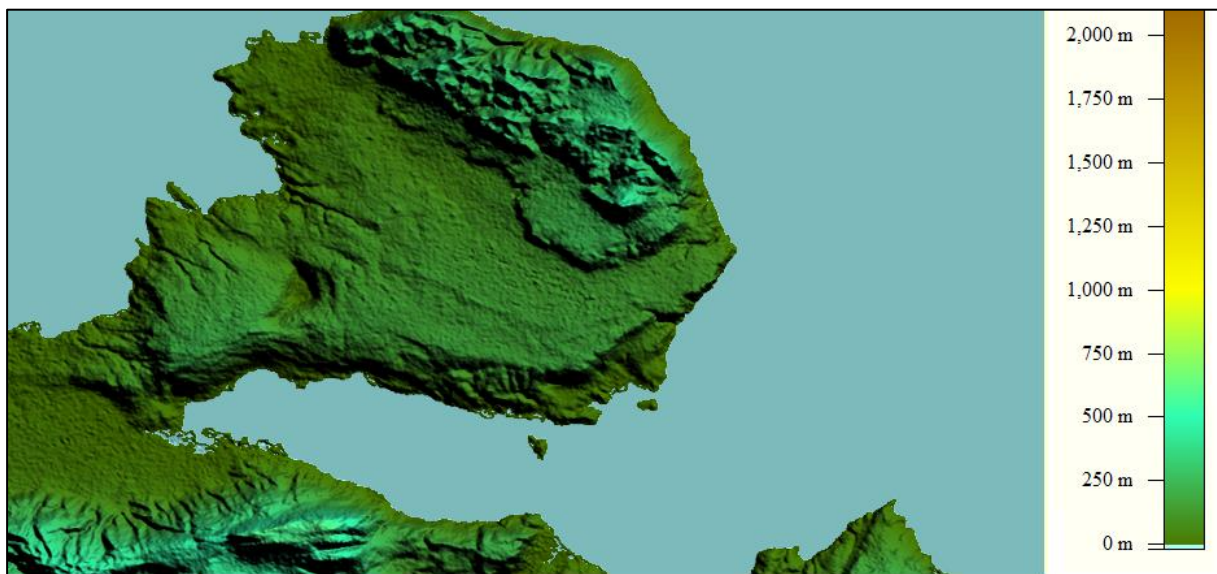

Figure 3.3: Studied area geographical characteristics (viewed with Global Mapper).

The delineation of the land portion of the studied area has been carried out in MatLab environment (R2014b). Therefore, a dedicated code has been developed to produce the shoreline. The output file from AERMAP preprocessor which included the coordinates of the receptors has been used for this purpose. Since the receptors have been distributed in AERGRID preprocessor with a spacing of 200m, the precision of the created shoreline in the map has a resolution of 200m.

The constructed map has been used as a canvas so the dispersion models could be super positioned. Both latitude and longitude coordinates have been expressed in UTM [m]. The map incorporates a grid which defines 24 square blocks of 16km^2, since both latitude and longitude axes have been divided into 4km intervals. Moreover, the intersection of the middle distances of the two axes coincides with the center of the main runway. Finally, the airport main runway is depicted as a black color line in the map. The constructed map is shown in Figure 3.4.
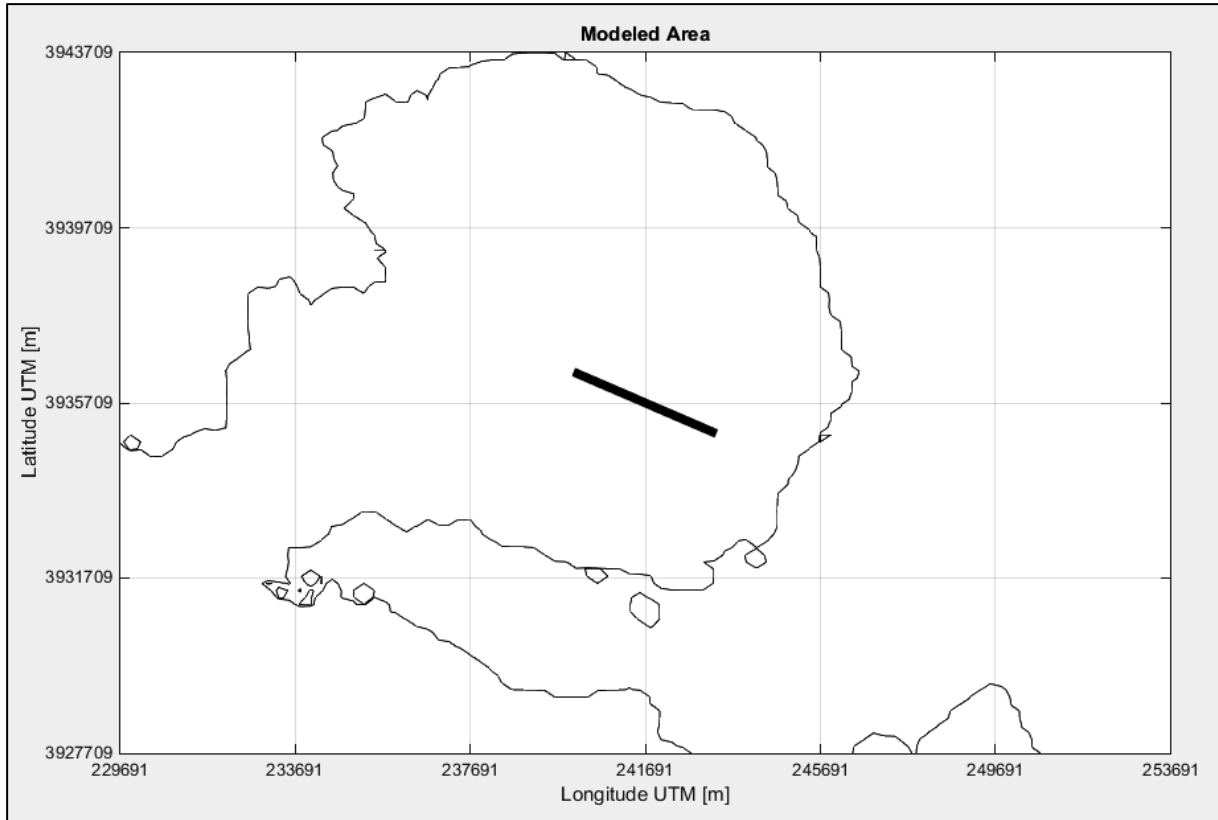
Figure 3.4: Studied area of Akrotiri (airport actual position is shown in black).

3.2. Meteorological Data

The weather station of Chania Airport is coded as 16746 according to World Meteorological Organization (WMO) [29]. The required meteorological data for the conduction of this study included wind data, i.e. direction [degrees] and speed [m/s], barometric pressure [mb], dry bulb temperature [^{o}C], relative humidity [%], precipitation [mm/hr] and total cloud cover [tenths]. Wind data have been provided from a meteorological site [29], whereas the rest data have been provided from the Hellenic National Meteorological Service (HNMS) through a personal request.

Hourly measurements of wind data for the year 2016 are shown together in the windrose diagram of Figure 3.5. As regards wind directions, it can be noticed that there has been a prevalence of North West direction by a percentage of 13%. The second dominant direction was West North West by 10,5%, while the third one was North by 8%. The predominance of the first two recorded wind directions justified an exclusive westward runway use option, in this study.

Wind speed has been separated into five intervals according to the legend of Figure 3.5. The first interval, i.e. [0,6 , 3,4) m/s possessed the 29% of the speed measurements and the

second one, i.e. [3,4 , 5,3) m/s possessed the 22% of them. Only 2,4% of the speed values were sorted above 9,9 m/s, whereas calms occupied the 27% of the measurements.
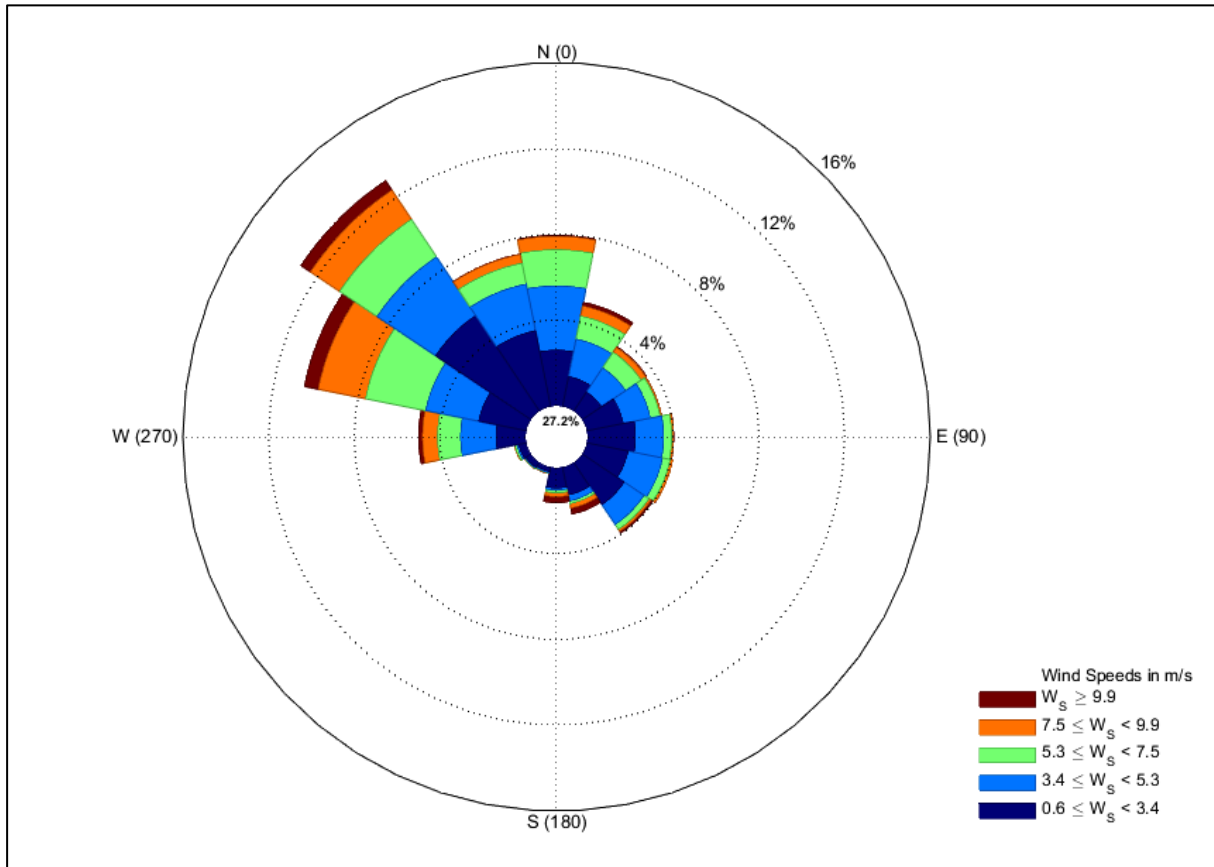

Figure 3.5: Wind profile of Chania Airport during the year 2016.

3.3. Emissions Sources

The emission sources of the airport have been initially declared in AERMAP preprocessor and they have been fully processed in AERMOD. Five separate emission sources have been defined in order that the typical LTO cycle could be modeled. Consequently, since every emission source corresponded to each different LTO phase, the number of the emissions sources was equal to the number of LTO phases, i.e. five.

All of the source types have been declared as area sources. According to the wind profile of the airport, which showed that there has been a predominance of mainly North West and secondarily West North West winds, the emission sources have been set-up under the acceptance that the majority of the aircraft movements had been carried out using the "29" runway option. Starting from the parking area, the aircrafts have been taxiing-out moving South East via the North East taxiway, taking-off using the "29" runway and climbing out up to 3.000ft. Similarly, after descending from 3000ft, they have been approaching and landing

moving North West, and taxiing-in the parking area. This scenario is provided in Figure 3.6 along with the defined emission sources.
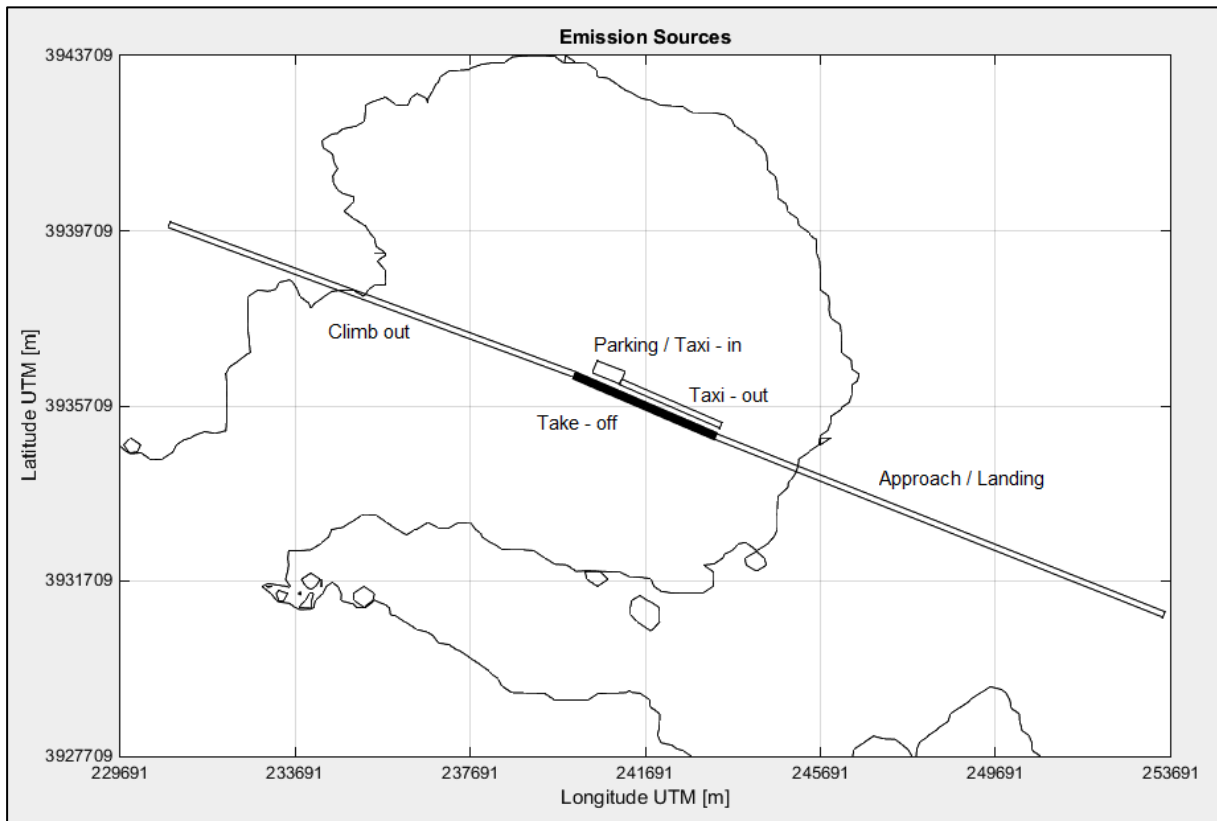

Figure 3.6: Emission sources of the model.

The emissions sources which refer to take-off, taxi-in and taxi-out have been regarded as ground level sources, thus their pollutants' release height has been set to 2m above the ground, which is technically an average height of the aircrafts engines exhausts. The consideration of climb out and approach/landing area sources opposed the fact that the release height is not steady during these phases due to the respective aircrafts constant loss or gain of flight altitude. Therefore, the release height for these emissions sources has been placed at the altitude level of 1.500ft, which is the average altitude between 3.000ft and the ground.

Despite this acceptance, the emissions produced from these sources proved of little contribution to the total pollution model. Numerous test runs have been conducted by lowering the release height below 1.500ft, even to 300ft, with small differentiations on the results. This is explained by the fact that these two sources provide a very large area for the emissions to disperse. The loss of this amount of emissions produced in these two phases, has been compensated for by the emissions produced in take-off source, since there has been the acceptance that the aircrafts use all the available runway length in order to become airborne.

3.4. Emissions Receptors

Apart from the sources setup, the determination of the receptors is also mandatory for the AERMAP run. The site of interest has been regarded as a rectangular area of 384km^2, since the length of the area was 24km and its width was 16km. It must be noted that AERGRID input file requires that the greater dimension is considered width and the smaller length. The distribution of the receptors followed a spacing of 200m, so their total number reached 9.600. However, AERMAP produced 9.801 receptors, 5.584 of which were on the sea level, 4.202 were above sea level and 15 were below sea level, proving that the percentage of sea coverage is about 57% while the land coverage is 43% of the examined area.

Elevation data have been acquired through the USGS official site [28] as a geotiff file format. With both the elevation data set and the receptors locations available, the AERMAP preprocessor produced the 3D coordinates of the receptors. In other words, the "receptors net" created through the AERGRID, has been super positioned on the DEM file. The receptors vector has been inserted to Matlab R2014b, and after the appropriate handling via a dedicated code, the plot of the coordinates is presented in Figure 3.7. The dimensions of the observed squares in Figure 3.7 are 200m by 200m, indicating that the distance between successive receptors is indeed 200m. All the line intersections in Figure 3.7 represent a receptor location.
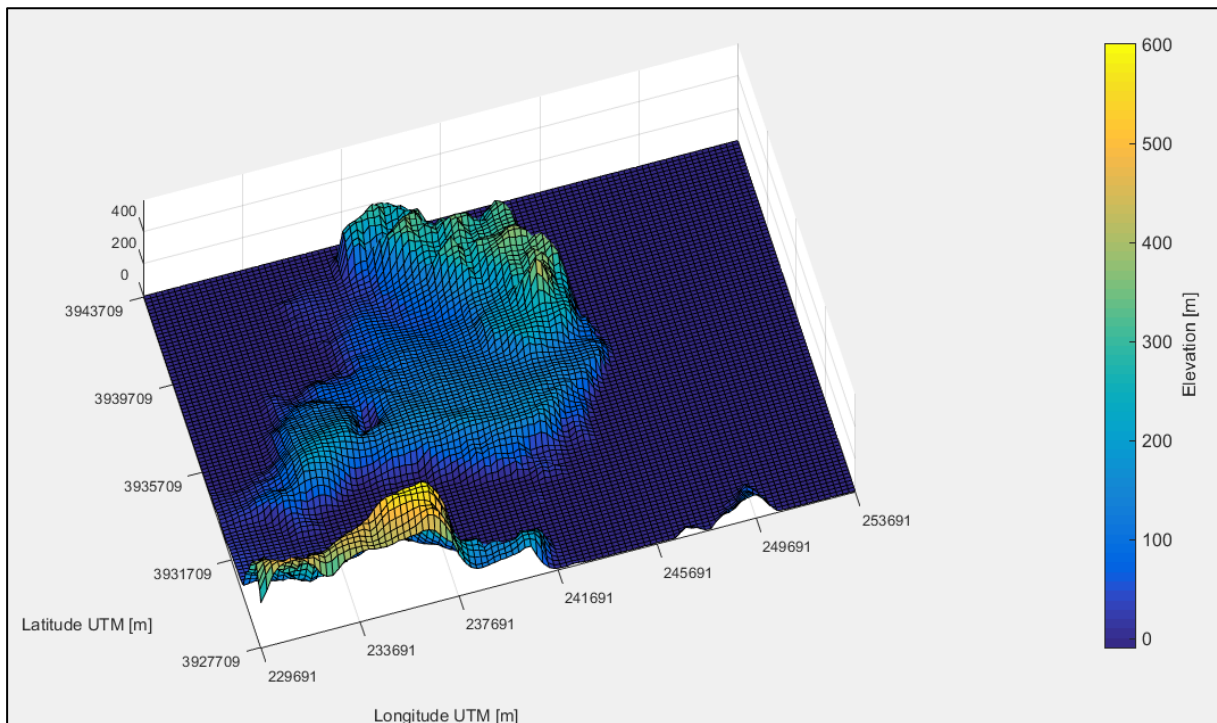

Figure 3.7: Distribution of receptors with a spacing of 200m at the studied area.

3.5. Traffic Composition

Throughout the year 2016, Chania Airport serviced 135 different types of aircrafts which performed 10.324 LTO cycles. However, the frequency of occurrence was not the same for all these aircrafts. The composition of the air traffic has been determined with traffic data provided by the HCAA, and it is given in Figure 3.8.
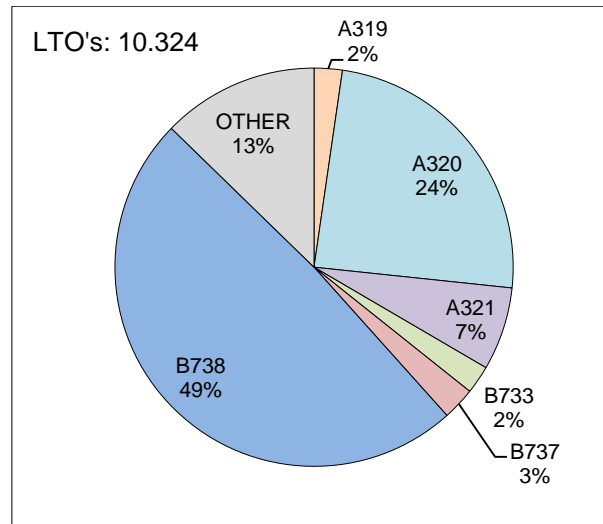

Figure 3.8: Air traffic and air traffic composition in Chania Airport for the year 2016.

Although the number of aircrafts was quite large (135), the majority of LTO cycles have been performed by only 6 aircraft types that occupied 87% of the traffic composition. The remaining 13% refers to the group of aircrafts with a relatively small presence (below 180 LTO's) in the whole traffic load. Boeing aircrafts occupied over 50% of the traffic, since 737-800 had the biggest share of the flight activity (49%). On the other hand, Airbus aircrafts had the second largest traffic portion with a total of 33%.

The group which is entitled as "OTHER" in Figure 3.8 incorporates 129 different aircraft types with a very small presence in the airport which was below 2% of the traffic. This significant fragmentation suggested a collective consideration of these aircrafts. However, the most common aircraft in this category was 767-300 occupying a percentage of 1,7% of the traffic. For this reason, the group "OTHER" has been regarded as a portion with exclusive presence of 767-300 aircrafts.

3.6. Aircraft Engines

The overview of the traffic composition for the year 2016 proved that there were 7 aircraft types characterizing the total flight activity of the airport. Air pollution calculations have been carried out by matching every aircraft type with the respective engine model according to [30]. The number of engines which is also an input parameter for the pollution equations was

found also in [30]. Table 3.1 provides engines data for the 7 most frequently recorded aircraft types at Chania Airport.

Table 3.1: Engines data of the most common aircrafts operated at Chania Airport during 2016.

ICAO Code	Description	Number of Engines	ICAO Engine Model
A319	Airbus A319	2	CFM56-5A5
A320	Airbus A320	2	CFM56-5A1
A321	Airbus A321	2	CFM56-5B3/P
B733	Boeing 737-300	2	CFM56-3B-1
B737	Boeing 737-307	2	CFM56-7B22
B738	Boeing 737-308	2	CFM56-7B26
B763	Boeing 767-300	2	PW4060

3.7. Emissions Calculations

The present study has evaluated the effect of civil aviation aircraft activity on local air quality by estimating and modeling four pollution species, i.e. carbon monoxide (CO), nitrogen oxides (NO_X), particulate matter with aerodynamic diameter 2,5μm or less (PM 2,5) and sulphur oxides (SO_X). Particulate matter from exhausts of modern aircrafts has an aerodynamic diameter of 0,1μm or less [31] [32] [18]. Since the particulate matter of this class is not monitored by the Directive 2008/50/EC, the next size class of PM 2,5 has been selected to be examined in this study. Carbon dioxide (CO_2) has also been included due to its contribution to the climate change. It is mentioned that the results originate exclusively from LTO cycles, since the emissions from aircrafts' auxiliary power units (APU's) have not been studied. Emissions from support and passenger vehicles inside and near the airport have not been studied either.

Emissions have been calculated according to the simple approach (option B) reported in [30]. A more generalized form of this approach includes the total activity of all different aircraft types operated in the studied airport, which is mathematically expressed by Equation (3.1).

$$Ei = \sum_{j=1}^{m} A_j \times \sum_{k=1}^{p} TIM_{jk} \times FF_{jk} \times Ei_{ijk} \times Ne_j \tag{3.1}$$

where:
Ei : total emissions of pollutant i produced by all aircraft types [g];
j : aircraft type;
m : total number of aircraft types operated in the airport;
k : LTO mode (approach/landing, taxi-in, taxi-out, take-off, climb out)

p : total number of LTO modes (i.e. five);

A_j : total activity of aircraft type j [LTO's];

TIM_{jk} : time-in-mode for mode k for aircraft type j [s];

FF_{jk} : fuel flow for mode k for each engine used on aircraft type j [kg/s];

Ei_{ijk} : emission index for pollutant i in mode k for engine used on aircraft type j [g/kg of fuel];

Ne_j : number of engines used on aircraft type j;

Emission rates for the AERMOD input have been calculated by isolating the emissions produced from each source during the respective sum of LTO's modes. These emissions have been divided by both the studied period, i.e. one year, and the emission source area where the LTO modes have taken place. Consequently, the emission rates are given by Equation (3.2).

$$Er_i = \frac{\sum_{j=1}^{m} A_j \times TIM_{jk} \times FF_{jk} \times Ei_{ijk} \times Ne_j}{Et \times Es} \tag{3.2}$$

where:

Er_i : emission rate of pollutant i produced by all aircraft types during LTO mode k [g/(s·m$^{2)}$];

Et : total time of studied period [s]

Es : emission source area [m^2]

Airport traffic data for the year 2016 has been provided by the State Aviation Authority at Chania Airport. Apart from taxi in and taxi out times which have been provided through personal communication with the mentioned Authority, standard ICAO modal times have been used for the rest of the LTO phases, i.e. approach and landing, take off and climb out. The duration of a typical LTO cycle at Chania Airport is 1.649s (27,48min). The entire set of modal times, is given in Table 3.2.

Table 3.2: Chania Airport LTO cycle modal times (data for modes 1,4 and 5 provided from [30]).

	Mode	Time-in-mode [s]
1	Approach/Landing	240
2	*Taxi in*	*616*
3	*Taxi out*	*619*
4	Take off	42
5	Climb out	132

The required engines data i.e. fuel consumption and emission indices, have been selected from ICAO Engine Emissions Data Bank [33]. ICAO document 9889 [30] provided information about the respective power plant that the involved aircraft types are equipped with, along with the number of engines of each aircraft type.

Emission indices for CO and NO_X have been taken directly from ICAO Engine Emissions Data Bank. Emission indices for CO_2 have been calculated by taking into account that 3,16 kg of CO_2 are emitted for every kg of consumed jet fuel [34]. Emission indices for SO_2 have been determined considering that S content in fuel is 0.05%. Since the molar mass of SO_2 equals two times the molar mass of S, the emitted SO_2 has been calculated to be 1 g for every kg of consumed jet fuel [34] [30] [31].

ICAO Engine Emissions Data Bank does not include data regarding particulate matter (PM), also. However, the detailed methodology i.e. First Order Approximation (FOA version 3) which is provided in [30] has been used for the construction of emission indices for this pollutant. Several engine technical characteristics such as smoke number (SN), by pass ratio (BPR) and air to fuel ratio (AFR) were used for the calculations. SN and BPR have been selected from [33], whereas default LTO values for AFR have been provided from [30].

The implementation of Equation (3.2) produced the emission rates for the AERMOD input expressed in grams per $(s \cdot m^2)$, and they are given in Table 3.3.

Table 3.3: Pollutants emission rates for AERMOD input $(g \cdot s^{-1} \cdot m^{-2})$.

Phase	CO	NO_X	CO_2	SO_2	$PM_{2.5}$
App./Land.	1,3322E-07	7,34927E-07	0,000221451	7,00793E-08	5,17145E-09
Taxi in	5,24308E-06	1,24011E-06	0,000856715	2,71112E-07	4,99743E-08
Taxi out	1,33309E-05	3,15306E-06	0,002178249	6,89319E-07	1,27063E-07
Take off	1,11229E-07	7,24778E-06	0,000783099	2,47816E-07	4,0645E-08
Climb out	1,41683E-07	4,78828E-06	0,000667513	2,11238E-07	1,46006E-07

3.8. Meteorological Calculations

Instead of an AERMET preprocessor run, the output surface (.SFC) and profile (.PFL) files have been designed from scratch in this study. Consequently, the involved parameters had to be selected or calculated according to the analytical methodologies which are provided in [35]. Additional information for the calculations can be found in [36]. These calculations required several primary meteorological data. Hourly wind direction and speed were provided

from [29] whereas barometric pressure, dry bulb temperature, relative humidity, precipitation and total cloud cover have been provided from HNMS (see §3.2).

Vertical potential temperature gradient (VPTG) above height of convectively-generated boundary layer (Zic) has been set to 0,013 K/m according to [37]. Surface roughness length (z_0) has been considered 0,5m and Bowen Ratio (B_0) has been set to 1,5 by taking into account the specific terrain and seasonal characteristics of the studied site, according to the classification provided in [35]. Reference heights for wind (z_{ref}) temperature (z_{temp}) have been set to 3m and 2m respectively due to the meteorological station distance from the ground surface. Stable atmosphere has been assumed for night hours while unstable atmosphere has been assumed during the day. A thorough description about the calculations for unstable and stable atmosphere is provided in Appendix A.

This page has been intentionally left blank.

4. Results

4.1. Emissions Estimation

The total number of LTO cycles performed by civil aviation aircrafts during the year 2016, was 10.324. The total annual fuel consumption inside the examined area reached 9.136t. The produced pollutants emissions were estimated according to the described methodology of §3.7. Total amount of emitted CO were estimated to be 66,4t and the emitted amount NO_X has been estimated to be 136,95t. Smaller amounts were estimated for PM 2,5 and SO_X which were calculated to be 2,976t and 9,136t, respectively. As regards the environmental interest for the climate change, annual CO_2 emissions reached 28.870t.

Division of the total fuel consumption to the total number of LTO's provides the information that 885kg of fuel were consumed per LTO at the airport during 2016. Division of the annual emitted amounts of SO_X and CO_2 to the consumed fuel yields 0,001 and 3,16, respectively. These numbers follow the acceptances under which the determination of the emission factors for these two pollutants have been carried out, i.e. for one kg of burnt fuel, 1g of SO_X and 3,16kg of CO_2 are emitted. Moreover, in terms of percentages, the emissions of CO, NO_X and PM 2,5 occupied 0,7%, 1,4% and 0,032% of the total fuel consumption, respectively. It can be concluded that the emissions of NO_X were two times greater than the emissions of CO.

The results that have been estimated for the emissions per every separate LTO phase suggest that CO has been mostly released during taxi-in and taxi-out phases. During taxi procedures, where engines' operation is in idle mode, the volumetric flow rate of air decreases so the fuel combustion is carried out under a lower AFR regime. Consequently, the combustion conditions favor the surplus of carbon contained in fuel which, in turn, increases the presence of CO in the exhaust gases. On the other hand, during the rest LTO phases, the engines' power settings are greater, the air intake increases and the CO emissions are more limited [38].

NO_X emissions have been noticeably increased during approach/landing, take-off and climb out compared to those during taxi-in and taxi-out. The explanation is similar to the CO emissions but in the opposite direction. Increased power settings during take-off and above-the-ground phases provide the engines with significantly greater amounts of air, so increased AFR's sustain a high surplus of nitrogen (N_2) in the combustion chambers. which is contained in the air by approximately 79% [38].

Given that air contains approximately 79% of N_2, the chemical reaction of fuel combustion ensures a high presence of N_2 in the combustion products. High temperatures inside the engines' combustion chambers favor the transformation of N_2 into NO_X which they are

released to the ambient environment with the exhaust gases [38]. Emissions of PM 2,5, SO_X and CO_2 simply follow the respective fuel consumption of every LTO phase. The calculated results are provided in Table 4.1.

Table 4.1: Annual aircraft emissions for each LTO phase (g/year).

Phase	CO	NO_X	$PM_{2.5}$	SO_2	CO_2
App./Land.	3.497.532	19.294.561	135.770	1.839.843	5.813.903.501
Taxi in	30.092.944	7.117.679	286.830	1.556.063	4.917.158.547
Taxi out	30.268.926	7.159.303	288.507	1.565.163	4.945.913.860
Take off	528.472	34.435.769	193.113	1.177.427	3.720.668.764
Climb out	2.010.645	67.951.387	2.071.997	2.997.723	9.472.803.542
LTO	66.398.520	135.958.698	2.976.217	9.136.218	28.870.448.215

The emissions results have been much lower than the emissions of a large airport in Turkey, i.e. Atatürk International Airport (AIA). The annual fuel consumption for the year 2015 in AIA was 277.492t and the released CO and NO_X emissions was 2.135t and 4.249t respectively [21]. Fuel consumption in Chania Airport during 2016 was 3,29% of the fuel consumption in AIA while the produced emissions of CO and NO_X in Chania Airport was 3,08% and 3,20% of the respective emissions in AIA. In terms of percentages, emissions CO and NO_X in AIA occupied 0,7% and 1,5% of the total fuel consumption, respectively. Moreover, NO_X emissions were about two times greater than CO emissions. Consequently, despite the large difference in absolute numbers between the two airports, the estimation methodology can be fully validated.

Another case study about Amerigo Vespucci Airport in Florence Italy showed that 25.588 flights during 2011 produced 50,75t of CO, 59,03t of NO_X and 5,39t of SO_X [22]. These results suggest that Chania Airport is of similar capacity in terms of both aircraft traffic and environmental impact. Despite the fact that the traffic in Florence Airport during 2011 has been approximately two times greater than the traffic in Chania Airport during 2016, the respective emissions were lower. This can be attributed to the different fleet composition between the two airports and the different meteorological conditions and geographical characteristics. However, the emissions are of similar size class.

Marco Polo Airport in Venice Italy is considered of the same interest compared to Chania Airport. Dividing the annual emissions of CO and NO_X released from Chania Airport during 2016 to the number of the year days, it can be assumed that the daily emissions of CO and NO_X were approximately 180kg and 371kg, respectively. The study of Marco Polo Airport, in

which two days of the year 2009 have been examined, showed that the daily emissions of CO and NO_X were approximately 1.270kg and 1.002kg, respectively [20].

4.2. Emissions Dispersion Modeling

Dispersion modeling has been carried out with EPA's AERMOD and the results have been compared to the regulated values described in the European Union Directive 2008/50/EC [3]. Pollutant species of SO_X and NO_X have been treated as SO_2 and NO_2, respectively. All the pollutants have been modeled according to the averaging periods mentioned in Directive 2008/50/EC [3]. Modeling of CO_2 has been examined on an annual averaging period in order to be evaluated for its contribution to climate change and related studies which have been conducted on an annual basis. The regulated values by 2008/50/EC [3] are provided in Table 4.2.

Table 4.2: Regulated values of common pollutants (data derived from [3]).

Pollutant	Averaging Period	Concentration [$\mu g/m^3$]
CO	Max daily 8 hour average	10.000
NO_2	1 hour	200
	1 year	40
PM2,5	1 year	20
SO_2	1 hour	350
	24 hours	125

As regards the technical details of the models, it must be mentioned that AERPLOT post-processor has not been used for the visualization of the results calculated by AERMOD. The values have been exported from AERMOD output files and they have been inserted to a dedicated code developed in Matlab R2014b, to produce the concentrations contours. The contours have been overlaid on the modeled area which has been also produced with a similar code. All of the pollutants' models hold that the airborne LTO modes have contributed little to the pollution of the area due to the significantly available space for dispersion of the emissions. On the other hand, ground operations have introduced most of the environmental impact in the area. First highest values have been modeled in all of the cases in this study. Aircrafts' emissions release has been considered exclusively upward and without the effect of the horizontal momentum of the exhaust gases [39].

4.2.1. CO Emissions Dispersion Model

Dispersion model of CO concentration for an 8 hour average has shown that the emissions have been kept at a low level compared to the value of 10.000$\mu g/m^3$. There has been an

accumulation at the North-West of the airport creating a zone of 200µg/m^3 around the aircraft's parking area and the end of runway with a highest value of 345,5µg/m^3. The modeled emissions of CO were quite close to the emissions measured at a large regional airport located in the West side of Romania [17], which has similar traffic capacity to Chania Airport. The measurements at this airport refer to a three day's period of June 2009 and they were conducted with three different devices at the aircraft's parking area. The results ranged between 250µg/m^3 and 700µg/m^3. The airport traffic for an 8 hour period was 35 aircrafts, while the daily average traffic of Chania Airport during 2016 was 28 aircrafts.

Chania Airport CO emissions during 2016 reached 3,08% of the respective emissions of Atatürk International Airport during 2015. The highest recorded modeled value there, was 19.839µg/m^3 [21]. Multiplication of the above percentage with 19.839µg/m^3, gives 611µg/m^3 which is not far from the value of 345,5µg/m^3 modeled in this study. Deviation can be explained given that meteorological conditions and terrain morphologies are different.

Emissions seem to comply with the wind profile of the area as the concentrations contours have an elongated form in parallel with the airport direction. The mountainous shelf of approximate elevation of 200m at the North-East of the airport suppresses the emissions near to the main runway, whereas the dispersion at the North-West of the airport is more unaffected by this natural obstacle. The dispersion model of CO is shown in Figure 4.1.
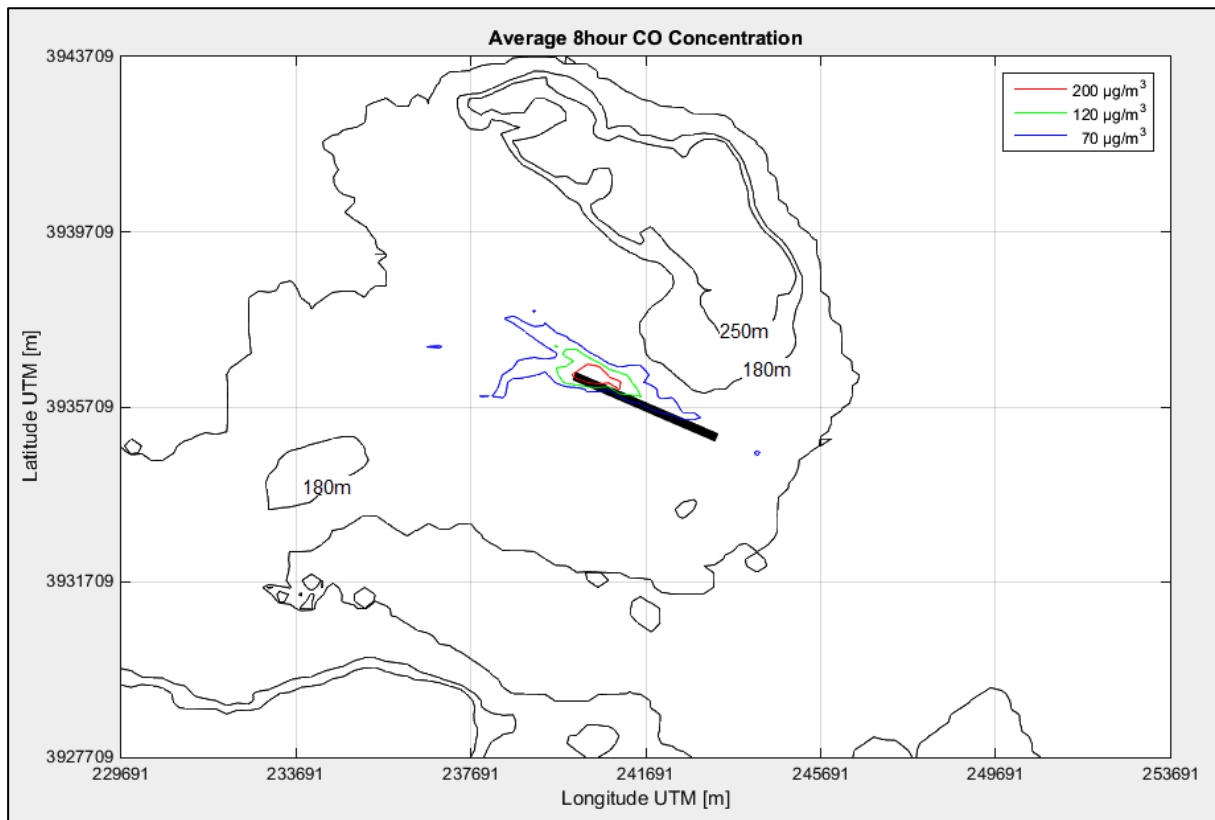

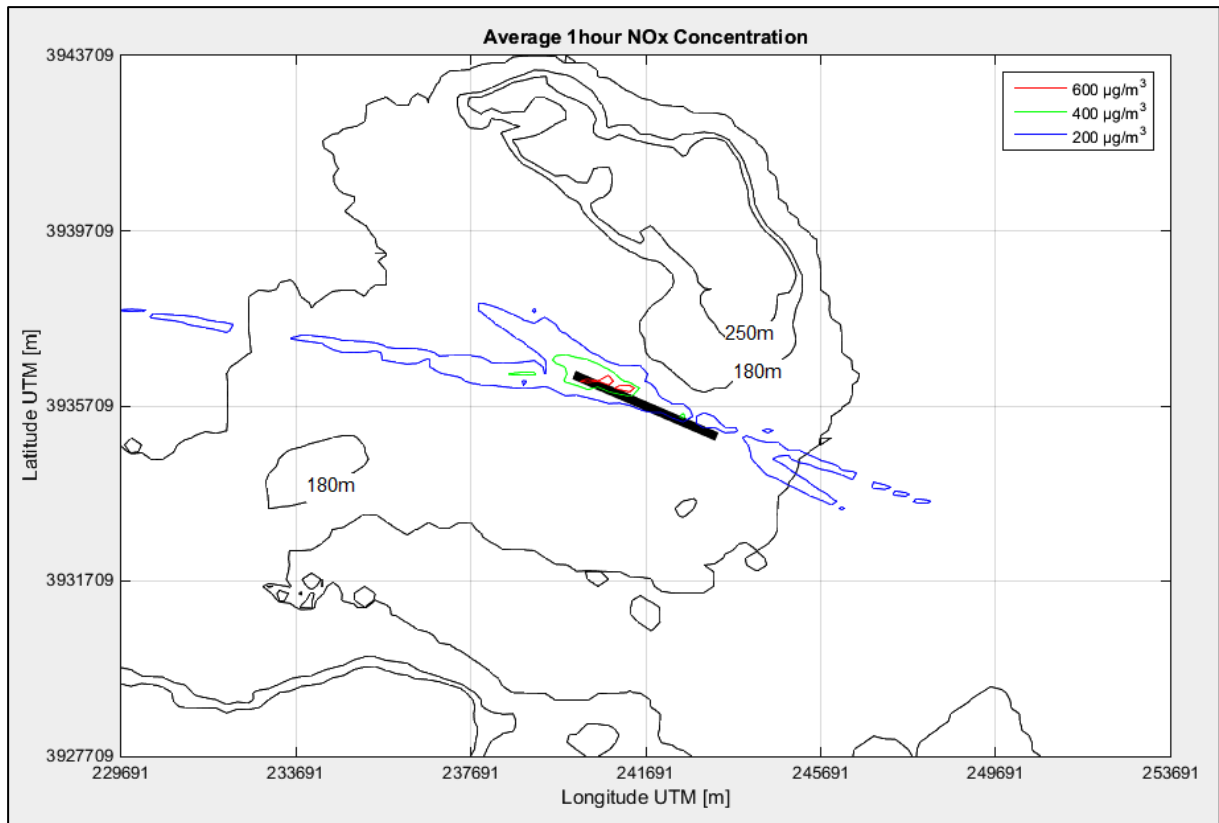**Figure 4.1:** Dispersion model of average 8 hour concentration for the year 2016 at Chania Airport.

4.2.2. NO_X Emission Dispersion Models

NO_X have been studied for the averaging period of 1 hour basis and for the annual basis. The model referring to the 1 hour average has revealed that emissions have been higher than the regulated value of 200µg/m^3. This threshold has defined a dispersion zone that expands in a great distance along the map. Segments of this zone have been transported even 12km at the West of the airport and 8km at the East. Sea level receptors in the east of the airport have been stimulated also, and a concentration contour which includes both land site and sea area has been formed, providing a confirmation of the three-dimensional structure of the model, considering the elevation difference of 150m between the airport and the sea level.
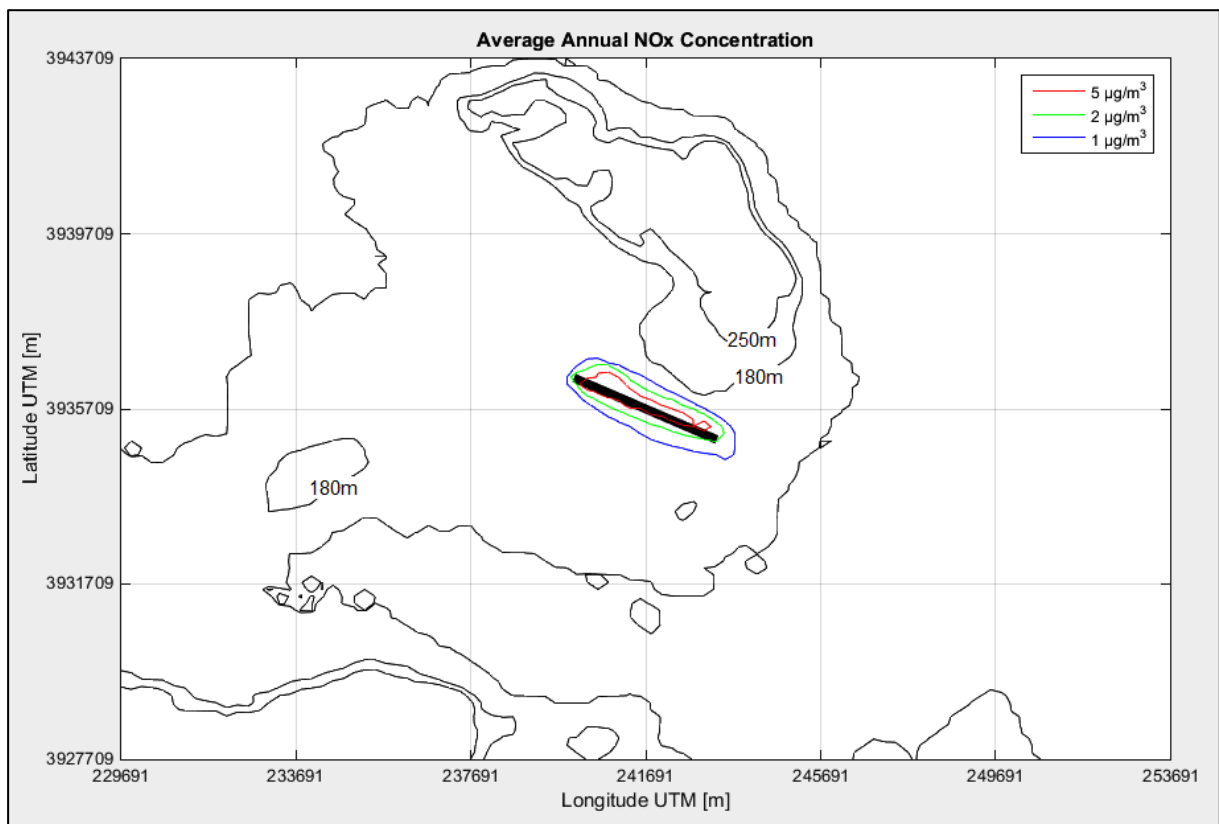
Inside the airport area, especially at the aircraft parking area and the North-West end of runway, NO_X concentrations have been much higher. In fact, emissions have created a zone of 400µg/m^3, i.e. two times the maximum regulated threshold value. Higher values of three times the threshold value have also been present forming the respective zones. Inside these areas the maximum value of 887,25µg/m^3 has been recorded. The mountainous shelf has restricted the dispersion from developing to the North-East of the airport.

Annual dispersion model revealed that the emissions have been very limited compared to the regulated value of 40µg/m^3. The annual dispersion model has a "tighter" form, since it seems to be more concentrated near to the airport. A zone of 5µg/m^3, i.e. 8 times lower than the maximum regulated value, spreads around the main runway and decays spatially to a zone of 2µg/m^3 and a zone of 1µg/m^3 as the distance from the airport increases. Inside the zone of 5µg/m^3, the maximum recorded value has been 18,09µg/m^3. The topographical anomaly at the North-East of the airport has not influenced the plume morphology to a significant extent.

The maximum concentration of 18,09µg/m^3 recorded in Chania Airport during 2016 has been 3,20% of the annual maximum value recorded in Atatürk International Airport during 2015, since the maximum modeled value at this airport has been 566µg/m^3 [21], proving that the relationship between the maximum concentrations at the two airports depends on the relationship between the respective total annual emissions. Annual NO_X emissions of 59,03t resulted in concentration values near to the regulated value of 40µg/m^3 at the parking area of Amerigo Vespucci Airport in 2011 [22]. The maximum concentration of NO_X (18,09µg/m^3) in Chania Airport has been also recorded at the parking area. However, the total emissions during 2016 were about two times greater than those in Amerigo Vespucci Airport during 2011. This discrepancy could be explained by the different aircraft fleet and the different meteorological conditions and the dispersion area terrain characteristics. The dispersion model of NO_X emissions is provided in Figure 4.2.

(a)

(b)

Figure 4.2: Dispersion model of average 1 hour (a), and annual concentration (b) for the year 2016 at Chania Airport.

Although 24 hour average concentration of NO_X is not monitored by any official regulatory context such the Directive 2008/50/EC, the respective model has been developed to provide comparisons with other studies. A study over Marco Polo Airport has shown that during two randomly selected days of the year 2009, the daily emissions of NO_X have been estimated to be approximately 1002kg [20]. The observed values of NO_X concentrations ranged from 10 to 120µg/m^3 at different sites of the airport.

The daily average of NO_X emissions in Chania Airport has been approximately 371kg, which can be translated to a percentage of 37%. The maximum concentration value according to the developed model of this study has been 70µg/m^3 at the North-West end of the main runway and there has been a zone of 50µg/m^3 around this peak value. In other words, the concentration profile of Chania Airport follows a percentage of 41% of the profile of Marco Polo Airport, which is close enough to the percentage of total emissions of NO_X. The 24 hour dispersion model is provided in Figure 4.3.
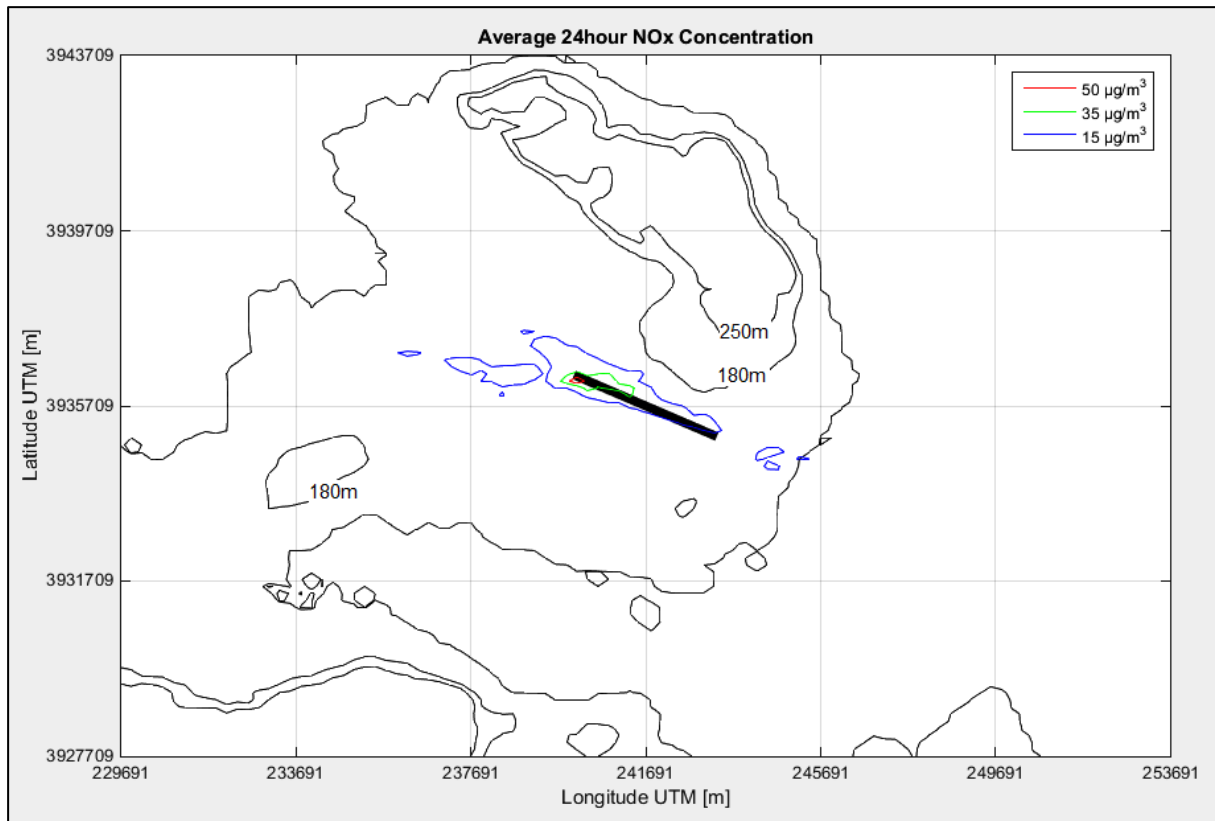

Figure 4.3: Dispersion model of 24 hour concentration of NO_X for the year 2016 at Chania Airport.
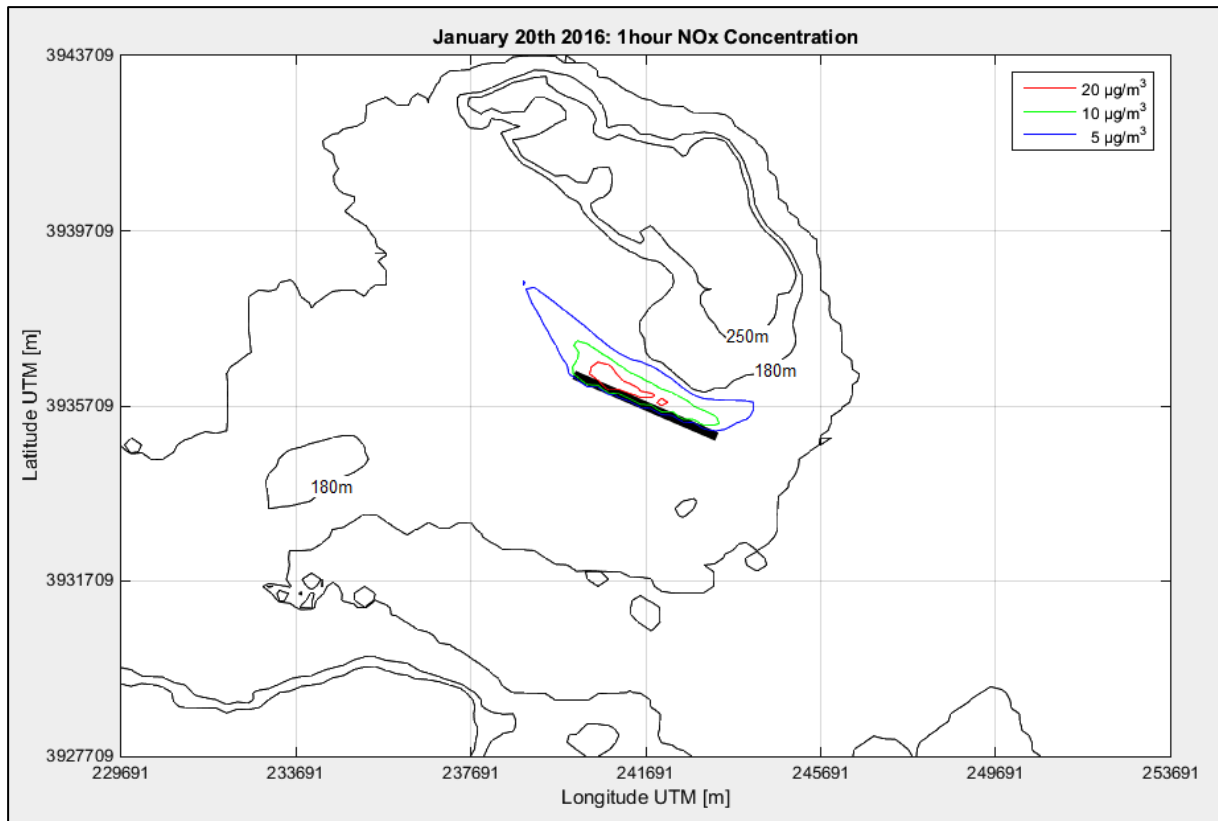
The described 1 hour model that had been produced over the annual basis of the year 2016 proved that the maximum value of NO_X has been approximately three times greater than the regulated value of $200\mu g/m^3$. The exceedance of the regulated value suggested that there should be further examination of the NO_X emissions. Therefore, two more models have been developed according to the described methodology in §3, in order to provide additional information about the environmental impact of this pollutant.

The first model refers to a randomly selected winter day, i.e. the 20th of January and the second refers to a summer day, six months later than the first one, i.e. the 20th of July. The selection was made given that the traffic data had been expected to be significantly different because of the charter flights during the summer period. In fact, according to the traffic data of July 20th, 123 LTO's were carried out during this particular day. On the other hand, traffic data of January 20th included only 16 LTO's, which means that the summer traffic was approximately 10 times greater than the winter traffic.
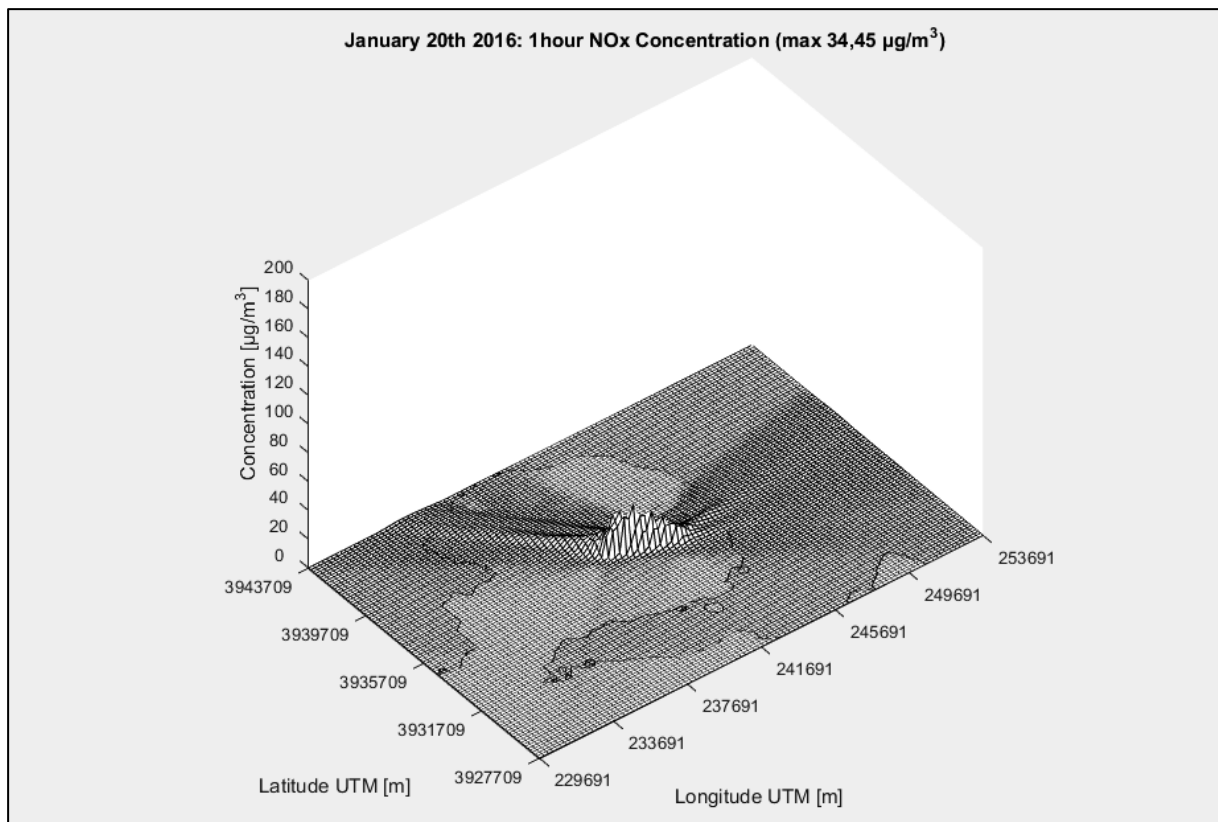
The aircraft fleet composition recorded during these two days simply follows the pattern of the annual fleet composition. In particular, Boeing 737-800's performed 6 out of 16 LTO's during the winter day and 47 LTO's during the summer day. An equal share of the summer day traffic was introduced by 767-300's with 47 LTO's, too. Airbus A320's performed 43 LTO's during the summer day.

The winter day model has shown that NO_X emissions have been approximately seven times below the threshold regulated value of $200\mu g/m^3$, with the maximum value of $34,45\mu g/m^3$ been recorded at the North-West of the airport. In this model the emissions are characterized by a limited dispersion concentrated mostly around the main runway and close to the airport. The wind regime mainly consisted of light winds and calm conditions (29,2%) have prevented the emissions from influencing the airport surroundings.

The summer day model has revealed that the emissions have exceeded approximately three times the regulated value of $200\mu g/m^3$. The maximum value of $546,11\mu g/m^3$ has been recorded over the main runway. The emissions have spread over the airport and there has been a secondary environmental concern as regards the neighboring sites on the East of it. Smaller fractions of the emissions have been transported via North-North West and North winds over Cretan Sea and Souda Bay, respectively where the sea level receptors have measured lower concentrations far below the threshold value. Calm conditions have been limited to 16,7% of the day measurements. A comparison of the two models is provided through Figure 4.4 and Figure 4.5 which include both top views and three-dimensional boxes of the concentration levels at the examined area.
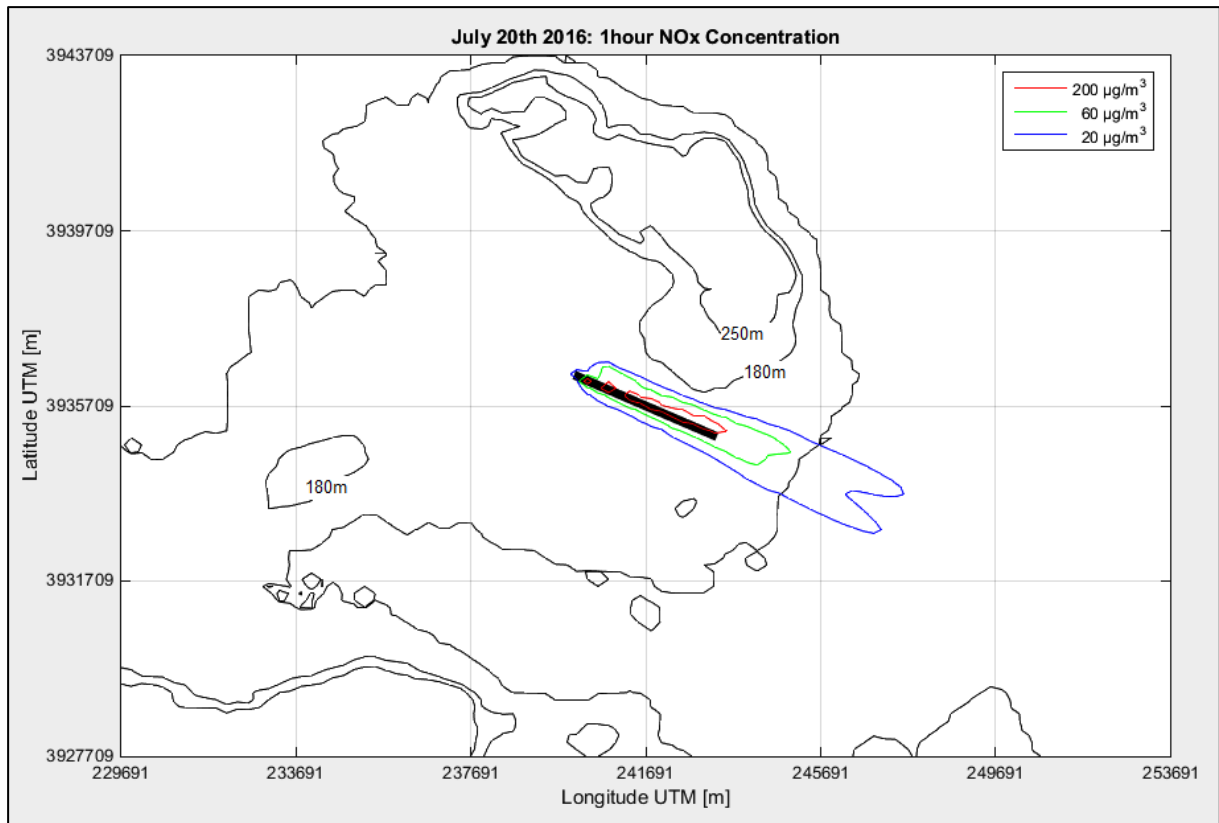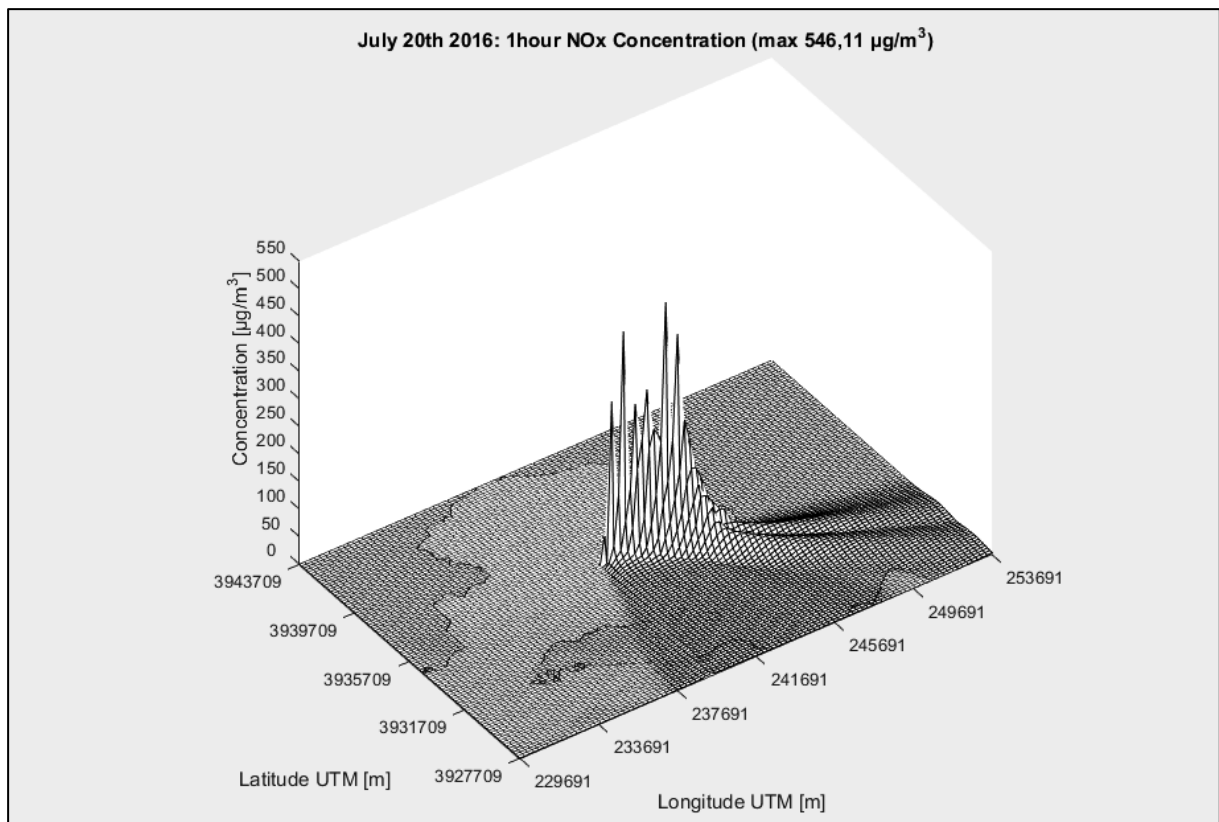
(a)

(b)

Figure 4.4: Winter day of 2016 dispersion model of NO_X at Chania Airport top view (a), 3d box (b).

(a)

(b)

Figure 4.5: Summer day of 2016 dispersion model of NO$_X$ at Chania Airport top view (a), 3d box (b).

4.2.3. Particulate Matter Emissions Dispersion Models

Emissions of PM2,5 refer only to annual basis according to the Directive 2008/50/EC. Dispersion model of this pollutant has shown that this species is not of major concern in the studied area. Recorded values have been significantly lower than the regulated maximum value of 20µg/m^3. The emissions have hardly exceeded the level of 0,3µg/m^3 since the maximum value has been 0,32µg/m^3 in the aircraft parking area.

A concentration zone of 0,2µg/m^3 which is one hundred times lower than the regulated value has been produced at the parking area. The dispersion has taken place in a uniform way which seems to be independent of the mountainous formation at the North-East. The dispersion model of average annual PM2,5 is provided in Figure 4.6.
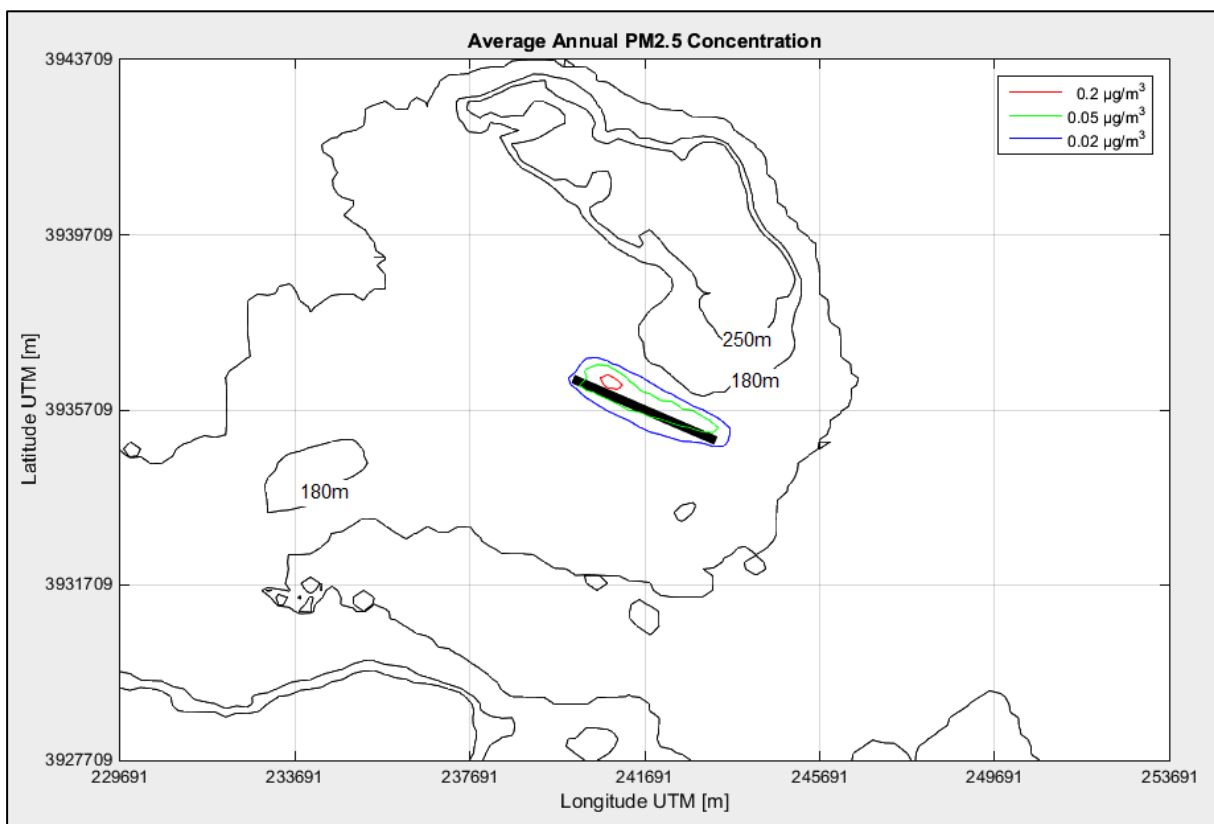

Figure 4.6: Dispersion model of annual concentration of PM2,5 for the year 2016 at Chania Airport.

A study over Los Angeles Airport concluded that the daily mean concentration levels of PM2,5 measured during five continuous 24h intervals in 2005, were between 32 and 42µg/m^3 [18]. Another study over the same airport revealed that PM2,5 concentration levels were approximately 33 µg/m^3 in a sampling period which included six randomly selected weekdays of May and July of 2016 [19]. In the first case 11 flights were recorded and monitored during 40 minutes, which implies that the daily activity of this airport was approximately 380 flights.

Given that the flight activity of Chania Airport during 2016 was approximately 28 flights per day, it can be concluded that the traffic at Chania Airport has been 7,3% of the traffic at Los Angeles Airport. This justifies that the maximum modeled 24 hour average concentration value of 1,23µg/m³ was about 3,8% of the respective maximum concentration that has been measured at Los Angeles Airport.

Despite the fact that the 24 hour average is not regulated by the Directive 2008/50/EC, the dispersion model for this time period has been also developed in order to assist in comparisons with other related case studies. The model is provided in Figure 4.7.
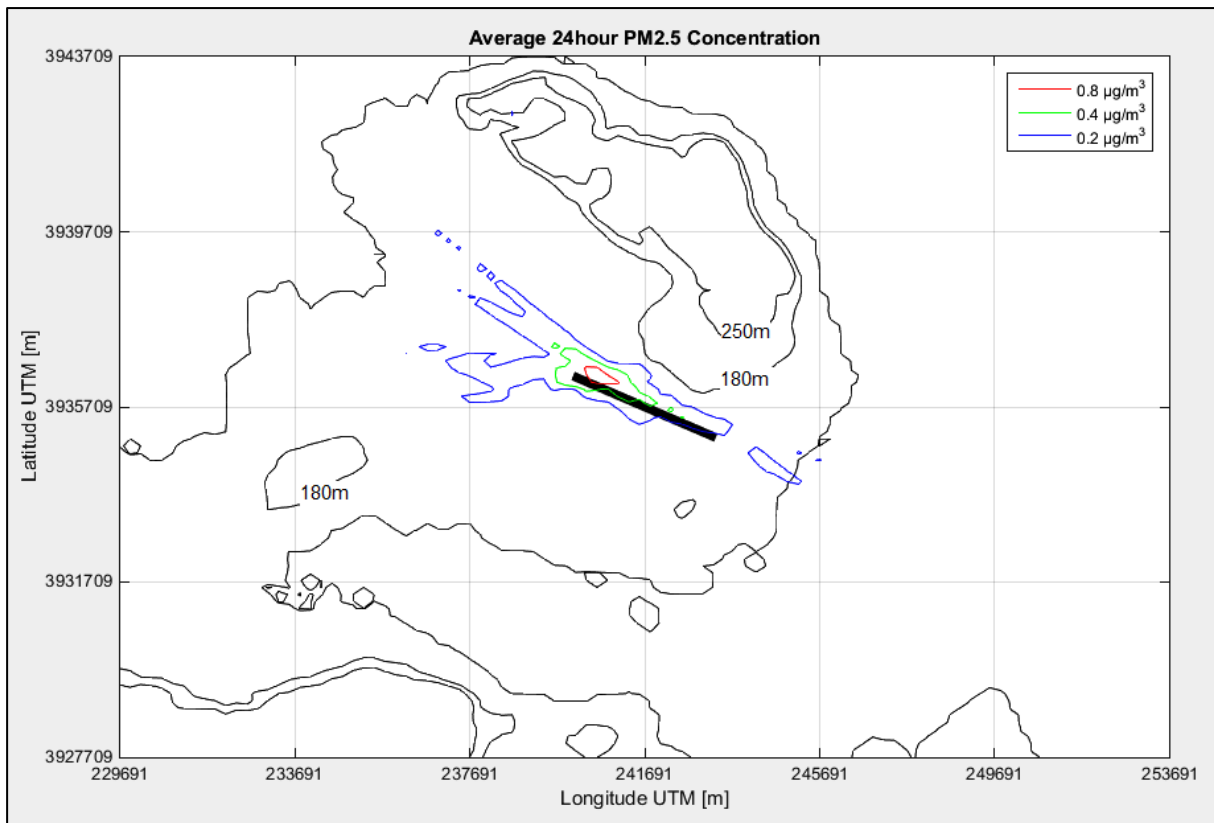

Figure 4.7: Dispersion model of 24 hour concentration of PM2,5 for the year 2016 at Chania Airport.

Technical details concerning the 24 hour concentration model of PM2,5 include mainly the dispersion morphology. As it can be clearly seen from Figure 4.7, the pollutant has expanded more freely to the West and North-West direction. Actually, the dispersion has been split to two separate formations which they have been expanded independently towards these directions. The elevated terrain at the north-east of the airport has played its role as a natural obstacle which has kept the pollutant from dispersing to the north direction.

Apart from the mass concentration, particulate matter has been modeled as regards its number concentration. The respective emission rates have been calculated according to the methodology described in §3. However, during the implementation of this methodology two

issues were raised. The first issue had to do with the fact that the emission factors data bases do not include emission indices for particles per unit of consumed fuel. Consequently, this type of emission indices had to be alternatively determined.

A related study has introduced a correlation between engine fuel consumption [kg/h] and the number of particles per kg of fuel burnt which is given by the Equation 4.1 [40].

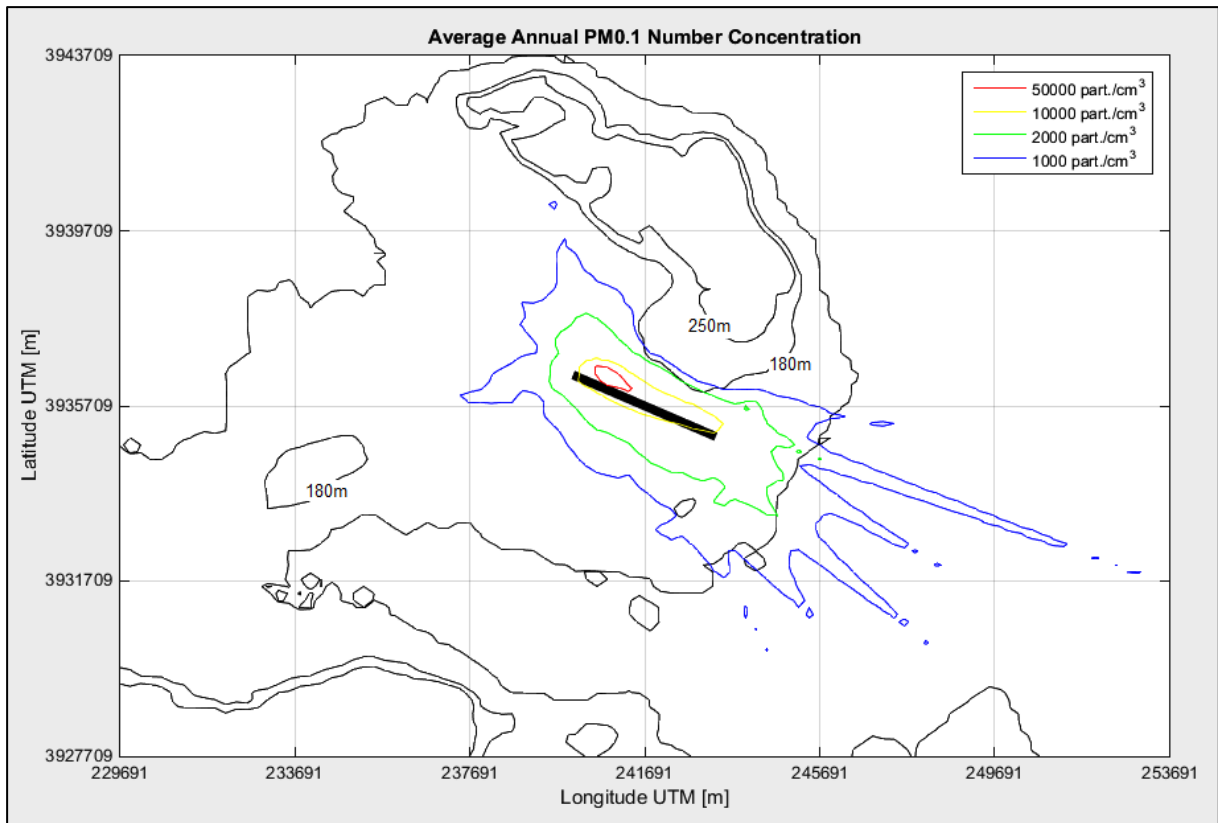$$EI_n = m \cdot \ln(\text{fuelflow}) + b \qquad\qquad (4.1)$$

where:
m : slope of the regression line;
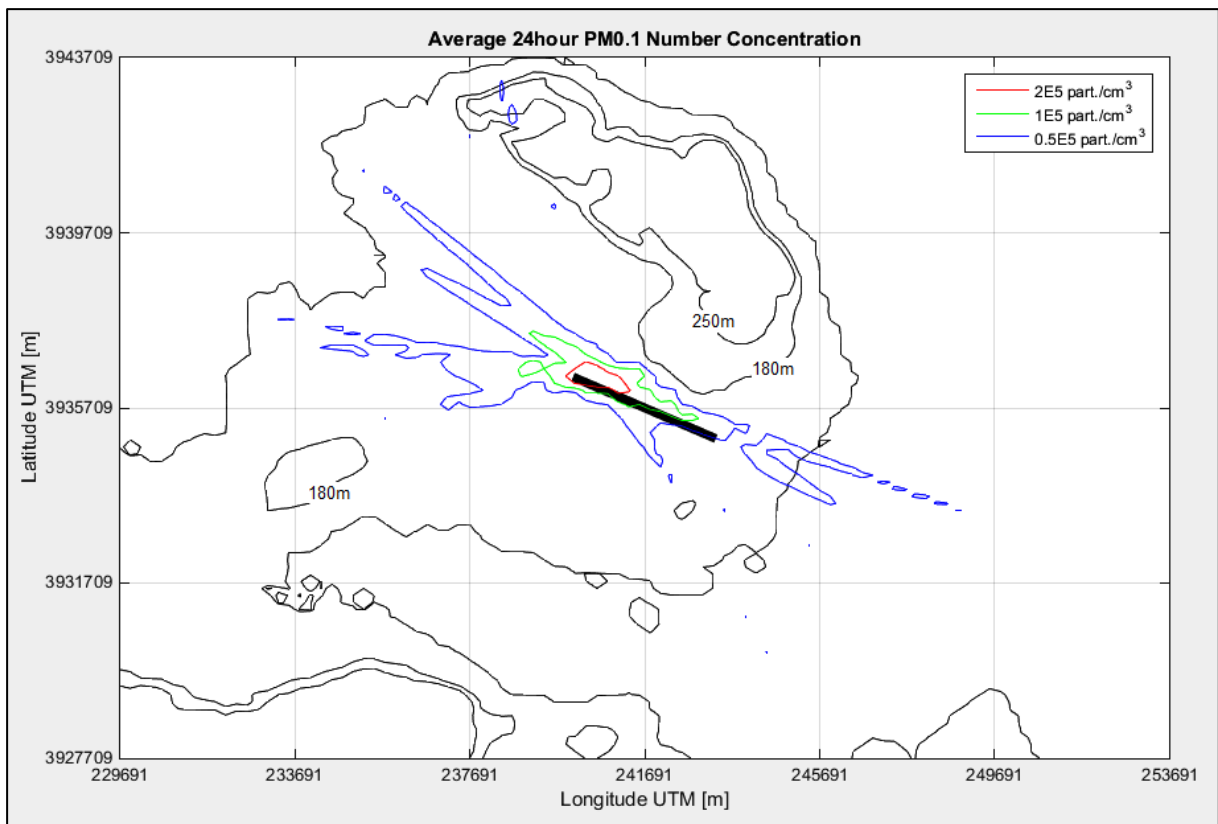b : intercept of the regression line;

Among the involved engines (see Table 3.1) the CFM56 ones have been treaded uniformly since they belong to the same technological group of CFM International turbofan engines. Therefore, the coefficient m of the Equation 4.1 has been set to (-2) and the term b has been set to ($2 \cdot 10^{17}$). Pratt and Whitney engine PW40600 (see Table 3.1) has been considered of the same technological characteristics as PW4158, so the coefficient m of the Equation 4.1 has been set to (-2) and the term b has been set to ($2 \cdot 10^{16}$). In both cases, the selection of the coefficient m and the term b has been made according to the experimentally determined values that are thoroughly described in [40].

The second issue had to do with the emission rate input units required by AERMOD and the desired output units. The common input unit for the emission rates required by AERMOD is [g/($m^2 \cdot s$)]. With this input unit, the output values that AERMOD produces are in [µg/m^3]. On the other hand, with the use of the described methodology in §3 and the implementation of Equation 4.1, the produced emission rates input units were [particles/($m^2 \cdot s$)]. Given that the desired output units had to be [particles/cm^3], the input values in [particles/($m^2 \cdot s$)] have been firstly multiplied by 10^{-12} in order to be operable when treated by the AERMOD internal functions.

Under these acceptances, two models have been developed for the number concentration of the particulate matter, one over the average annual and one over the average 24hour basis. The selected class for the particles for the input file of AERMOD has been PM0,1 since that the emissions from modern aircrafts exhausts contain exclusively ultrafine particles [18] [31] [32]. Both models of the ultrafine number concentrations are presented for comparison in Figure 4.8.

(a)

(b)

Figure 4.8: Dispersion model of average 1 hour (a), and annual ultrafine number concentration (b) for the year 2016 at Chania Airport.

In the first model, there has been a zone of 50.000 particles per cm^3 at the parking area with the maximum value reaching 111.190 particles per cm^3. Zones of lower concentrations have been created at long distances from the airport. The particles have been transported to the East of Akrotiri and the boundaries of a zone of 1.000 particles per cm^3 have reached the sea. This zone has been also expanded to the North but the mountainous shelf of 180m has acted as a natural obstacle for further expansion to the North.

As for the average 24 hour model, a zone of 200.000 particles per cm^3 has been created at the parking area. The maximum value of 428.830 particles per cm^3 has been recorded inside this zone. Moreover, a zone of 100.000 particles per cm^3 has been expanded around the main runway. The particulate matter has been transported mostly to the West of the airport creating zones of lower number concentrations, i.e. 50.000 particles per cm^3.

A recent study that was carried out at the international airport of the Greek island of Mytilene in 2014 concluded that the occurrence of ultrafine particles was strongly correlated to the aircraft flight activity, since the mean number concentration of the studied period reached 800.000 particles per cm^3 [41]. This value has been estimated through measurements that took place during six summer days, from July 24th to August 8th. A 24 hour model that was based on a 24 hour period of one single day, i.e. July 20th has been developed for Chania Airport for the need of comparisons, and it is presented in Figure 4.9.
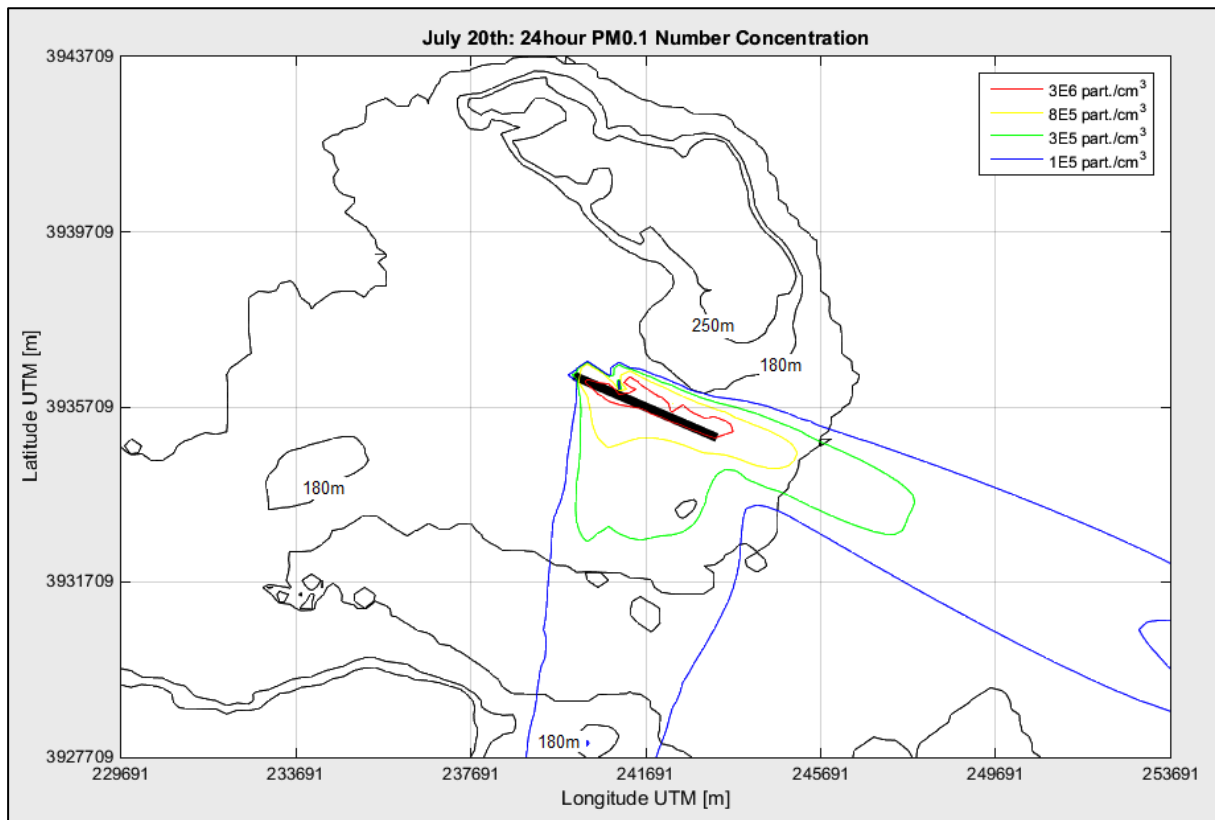

Figure 4.9: Summer day of 2016 dispersion model of ultrafine PM number concentration.

During July 27th of 2014, 13 flights were recorded at Mytilene Airport [41], while 123 flights were performed during July 20th of 2016 at Chania Airport. It can be generally said that Chania Airport has ten times the traffic of Mytilene Airport during summer days. According to the developed model, the maximum value of particles number concentration at Chania Airport has been 9.729.400 particles per cm^3, which is approximately ten times greater than the mean value of 800.000 particles per cm^3 at Mytilene Airport.
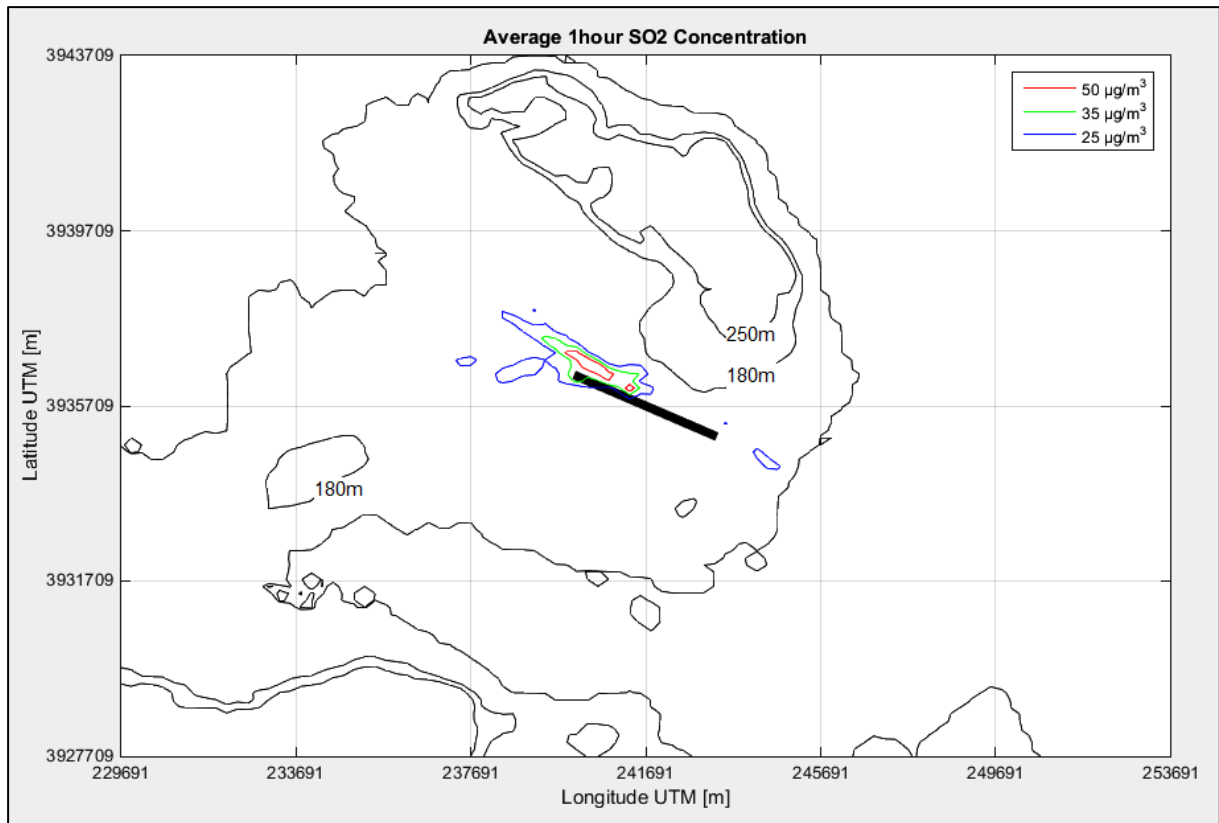
Supplementary information about this model can be provided through the interpretation of Figure 4.9. The particulate matter has been transported to the East of the airport and there is a zone of 100.000 particles per cm^3 that has split to two partitions. The first one has reached the Cretan Sea and the second one has even crossed Souda Bay and the pollutant have been deposited to the mountainous formation to the very South of the map at an elevation of 180m.

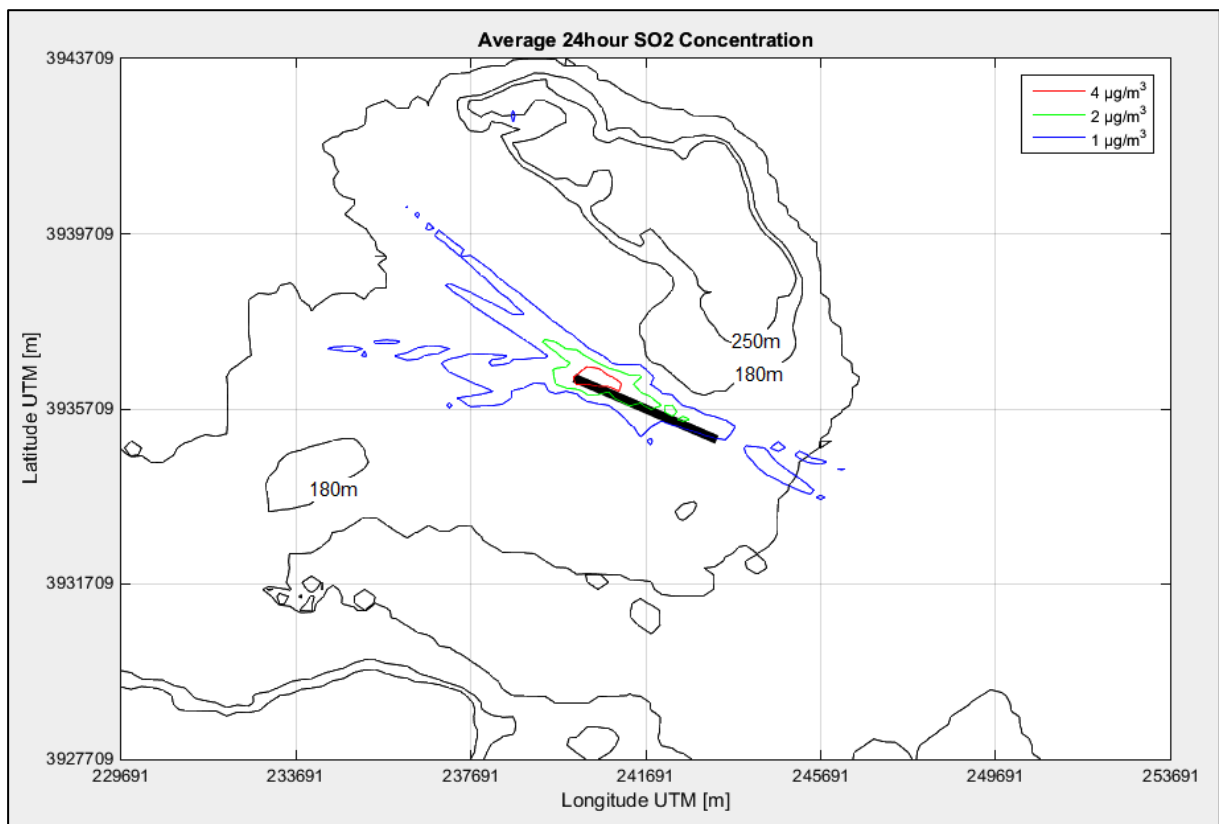### 4.2.4. SO$_X$ Emissions Dispersion Models

Emissions of SO$_X$ as SO$_2$ have been significantly lower than the regulated values described in the Directive 2008/50/EC. For the 1 hour average, the maximum concentration value has been 78,76μg/m^3 at the location of the parking area at the north-west of the airport which is approximately 22% of the maximum regulated value, i.e. 350μg/m^3. A concentration zone of 50μg/m^3 has been formed at this area which is followed by a spatial decay of the pollutant concentrations to lower values of 25μg/m^3. The dispersion has noticeably affected the north-west areas of the airport whereas the south-east areas have remained uninfluenced by this pollutant.

As regards the average 24 hour model, the maximum concentration of 6,7μg/m^{3}has been recorded at the North-West of the airport, also. This value has been only 5,3% of the maximum regulated value which is defined by the Directive 2008/50/EC. It is also mentioned that wet deposition of SO$_X$ has not been taken into consideration during the construction of AERMOD input file.

The average 1 hour concentrations have been comparable with the ones produced from an International Romanian Airport with similar traffic characteristics. The SO$_2$ emissions from this airport have not exceeded the level of 180μg/m^3 while the most common values ranged between 35 to 85μg/m^3 [17]. In general, the emissions of this pollutant comply both with the fuel consumption profile and the sulphur content in consumed fuel. The models for the regulated intervals are given in Figure 4.10.

(a)

(b)

Figure 4.10: Dispersion model of 1 hour (a), and 24 hours concentrations (b) of SO_2 for the year 2016 at Chania Airport.

4.2.5. CO_2 Emissions Dispersion Models

Emissions of CO_2 are not regulated by the European Directive 2008/50/EC. However, they are still monitored for their interference to the greenhouse effect (GHE). As a Member-State of the European Union, Greece has adopted and signed the Kyoto Protocol. It is interesting to examine the global impact of Chania Airport aircraft activity. According to the methodology discussed in §3.7, the total emissions of the airport during 2016, were 28.870t. In 2014, Greece was the 48th country in the global ranking of the year 2014 in terms of CO_2 emitted from fossil-fuel burning, cement production, and gas flaring, having released in the atmosphere 18.358.000t of carbon [42]. During 2014 Greece released (18.358.000×3,664)t of CO_2, i.e. 67.263.712t. Despite the different years of reference, division of the emissions of Chania Airport by this value provides the percentage of its contribution to the country's CO_2 emissions, which is about 0,043%. The dispersion model of CO_2 emissions is presented in Figure 4.11.

Figure 4.11: Dispersion model of annual concentration of CO_2 for the year 2016 at Chania Airport.

The dispersion model follows the orientation of the airport and the concentration zones expand in a uniform way around the main runway. As the rest pollutants the maximum zone has been formed at the North-West of the site and includes the aircrafts' parking area. Inside the maximum zone of 2.000µg/m^3, there has been recorded the highest value of the model which has reached 5.577µg/m^3.

5. Conclusions

Most of the dispersion layouts of the models give the impression that they follow the orientation of the airport (110° - 290°). This is explained by the wind profile which, in turn, is characterized by the predominance of West and North West winds at the examined area. There is a noticeable shape differentiation as regards the annual average models compared to the models developed on shorter average times, i.e. 24 hour, 8 hour and 1 hour. The latter are more elongated, the emissions are dispersed mostly along the main runway and they continue after the true horizon of the airport borders. On the other hand, the annual average models have a concentrated-to-the-airport form.

The explanation for this discrepancy can be attributed to the fact that AERMOD functions are based on the bi-Gaussian distribution in order to create the emissions dispersion models. Since the annual average models include meteorological data of the whole year, the wind directions are averaged on an annual basis and the spatial variance of the emissions distributions tends to be smaller. Shorter average times include meteorological observations of shorter time intervals and, consequently, the variance is greater since it is affected by the predominant conditions of the respective time interval.

The models have a three dimensional structure which is confirmed by the stimulated receptors spread on the three dimensional topography of the examined area. This is very obvious at the models other than the annual average, where the dispersion expands from the airport to the neighboring land site and, eventually, to the sea.

Apart from the meteorological conditions, the models are also affected by the terrain characteristics. The airport is located on a plain site of an elevation of 149m. The mountainous formation at the North-East of the airport and the shelf created by its foothills, favor the suppression of the emissions near to the airport. The dispersion is more limited in this direction due to the lack of available space. On the other hand, the dispersion is greater at the North-West where the mountainous formation is much more distant to the airport.

As regards the emission sources, the results have indicated that the aircraft ground operations have a greater environmental impact. The emission sources where the aircrafts are airborne have influenced the examined area to a negligible extent. These sources have occupied a great deal of area where the pollutants have been dispersed and the vast areas have favored the expansion of the exhaust gases. Eventually, the emissions have been prevented from concentrating close to the airport. Moreover, the release height for the above-the-ground operations has been set to 1.500ft, where the mean height of the LTO cycle is located. Thus, the receptors have not been able to receive any "signs" of pollution due to the relatively high level of the emissions' release height.

The methodologies used for both the emissions estimation and the determination of the emission rates have been cross-validated by examining the results of similar studies. The results of the present study, produced on certain airport traffic, seem to follow the traffic ratio of Chania Airport over the other examined airport, despite the significant traffic difference in absolute numbers. Moreover, the results have been validated with other studies which have incorporated dedicated techniques of field tests and measurements.

The results produced by the present study proved that the airport, as an emission source, introduces low levels of pollutions at the surrounding area. Except for 1 hour NO_X, all the other pollutant species have been proved to be of low environmental and health concerns. However, the airport emissions cannot be ignored because they can be correlated and added to other emission sources of the area. Emissions of NO_X can become the precursors of ozone which can also affect the local air quality.

The present study was carried out under the acceptance that the aircraft fleet composition had included 7 categories of aircraft types. Even though the seventh category has been denoted as B763, it has included 129 different aircraft types with a limited occurrence at the airport. There has been a big variety of different technologies as regards these aircrafts since their power plants have different principle of operation, i.e. gas turbines or reciprocating technologies. Different engines types require different fuel specifications (jet fuel or aviation gasoline) of different sulphur content, other than 0,05% that was used in this study. Future work could incorporate a full record of detailed fleet composition along with the differences in fuel type and, consequently, their different sulphur content which affects directly the emissions of SO_X.

Future work could also involve the study of the airport emissions, apart from the aircrafts LTO's. These emissions could refer to aircrafts secondary operations and their support equipment, such as onboard APU's and ground power units, along with the vehicle movements related to the aircrafts, such as refueling trucks and passengers transport vehicles. Moreover, there could be further study as regards the airports surroundings with the inclusion of the transport media of the passengers to the airport, i.e. buses, taxis and passengers vehicles, and the respective parking sites. Additionally, there could be further examination of emissions induced by fuel storage and sampling for quality assurance purposes, combustion facilities for heating and aircraft maintenance procedures such as corrosion prevention.

Finally, a holistic study of both the stationary and the mobile emission sources of the examined area could provide a more satisfactory evaluation of the environmental impact produced by the processes which accompany the anthropogenic activities. Such emission

sources of the area are the thermal power plant of Chania, the sewage treatment plant of Chania, the commercial port of Souda with the anchorage at the entrance of Souda Bay and the port of Agios Onoufrios [43] where a fuel storage and fuel transit facility is located, which also has an anchorage at the entrance of the port.

Moreover, urban and suburban combustion sources from the city of Chania and the nearby villages along with the road network could be studied with the implementation of other and more detailed methods like GIS since the complexity of these types of emission sources might exceed the capabilities of AERMOD. The most representative emission sources of the examined area are shown in Figure 5.1.
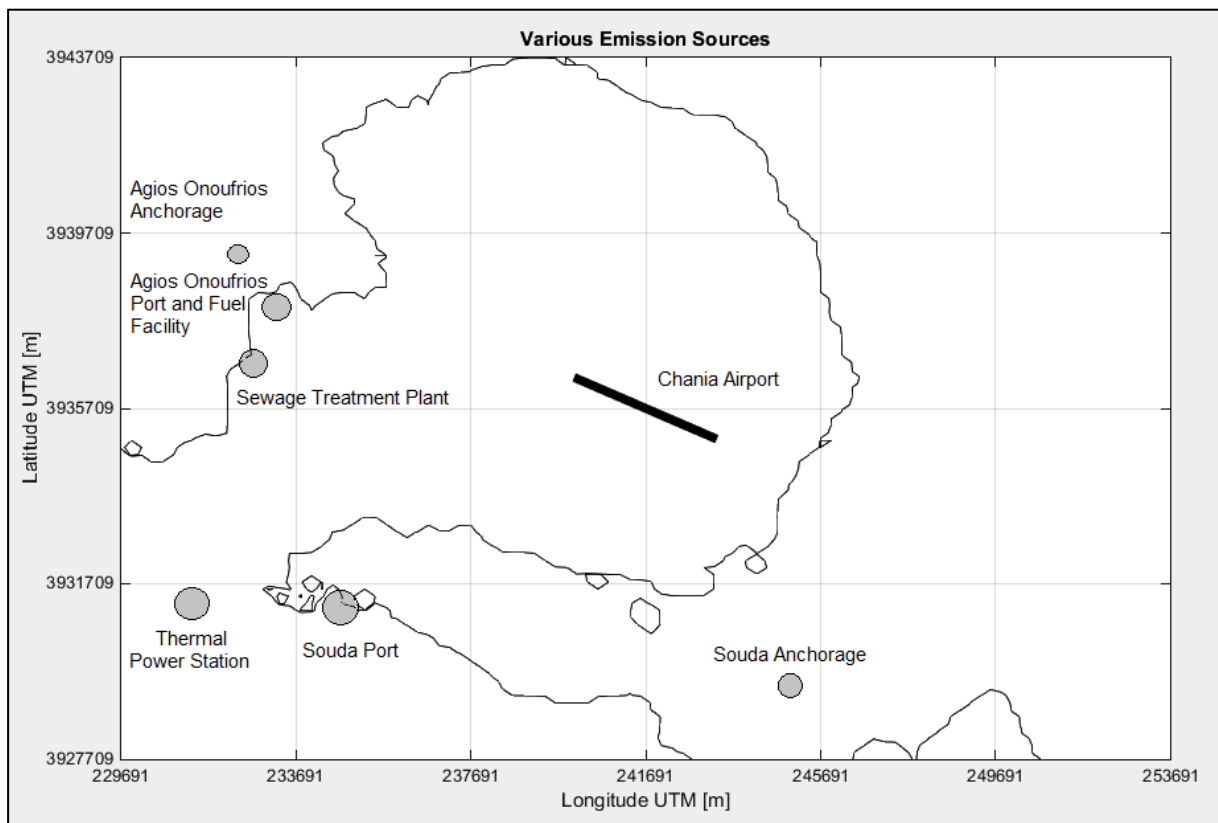

Figure 5.1: Other emission sources of anthropogenic activity inside the examined area.

This page has been intentionally left blank.

Appendix A - Methodologies for Unstable and Stable Atmosphere

A.1 Unstable Atmosphere

During daytime there is a positive heat flux from the surface to the lower air layer. This amount of heat is cumulative since the heat flux begins with the sunrise and seizes after sunset. The accumulation of heat sustains a convective boundary layer in which emissions can rise as the convective boundary layer height increases. As the emissions gain altitude through this process, the ground receptors are less stimulated, so the modeled values are smaller. In this study the estimation of the convective mixing height during daytime has been carried out numerically through the algorithm of Equation (A.1) [44].

$$\frac{dZ_{ic}}{dt} = (1 + 2 \cdot A) \cdot \frac{H}{\rho \cdot C_p \cdot \gamma_\theta \cdot Z_{ic}} + 2 \cdot B \cdot \frac{u_*^3 \cdot T}{g \cdot \gamma_\theta \cdot Z_{ic}^2} \tag{A.1}$$

where:

Z_C : convective mixing height for time "t" [m];

A, B : empirical constants (0,2 and 2,5 respectively);

H : surface heat flux [Watt/m^2];

ρ : density of air [kg/m^3];

Cp : specific heat of air at constant pressure [Joule/(kg·K)];

g : acceleration of gravity [m/sec^2];

γ_θ : potential temperature gradient above the mixing height (VPTG) [K/m];

u_* : friction velocity [m/sec]

T : reference temperature (on ground surface) [K]

The described methodologies from this point and on can be found in [35], [36]. Surface heat flux (H) has been calculated through the Equation (A.2).

$$H = \frac{0,9 \cdot R_n}{1 + \frac{1}{B_o}} \tag{A.2}$$

where:

R_n : net radiation [W/m^2];

B_o : Bowen ratio [set to 0,15];

Net radiation (R_n) has been calculated through the Equation (A.3).

$$R_n = \frac{[1 - r(\gamma s)] \cdot R + c_1 \cdot T^6 - \sigma_{SB} \cdot T^4 + c_2 \cdot n}{1 + c_3} \tag{A.3}$$

where:

σ_{SB} : Stefan-Boltzman constant [5,67×10^{-8} W/(K^4·m^2)];

c_1 : empirical constant [$5,31 \times 10^{-13}$ W/(K$^6 \cdot$m^2)];

c_2 : empirical constant [60 W/m^2];

c_3 : empirical constant [0,12];

r(γs) : surface albedo as a function of solar elevation angle (γs);

n : total cloud cover;

R : solar radiation corrected for cloud cover [W/m^2];

Solar radiation corrected for cloud cover (R) has been calculated through the Equation (A.4).

$$R = (990 \cdot \sin \gamma s - 30) \cdot (1 - 0,75 \cdot n^{3,4})$$ (A.4)

The surface albedo has been calculated through the Equation (A.5).

$$r(\gamma s) = r' + (1 - r) \cdot e^{\alpha \cdot \gamma s + b}$$ (A.5)

where:

α : 0,1;

b: $-0,5 \cdot (1-r')^2$;

r' : r(γs=90°)

Solar elevation angle for every hour throughout 2016 has been calculated according to the methodology presented in [45] (see Appendix B). The values have been processed in a spreadsheet and three characteristic days, i.e. winter and summer solstices and spring equinox are presented in Figure A.1.
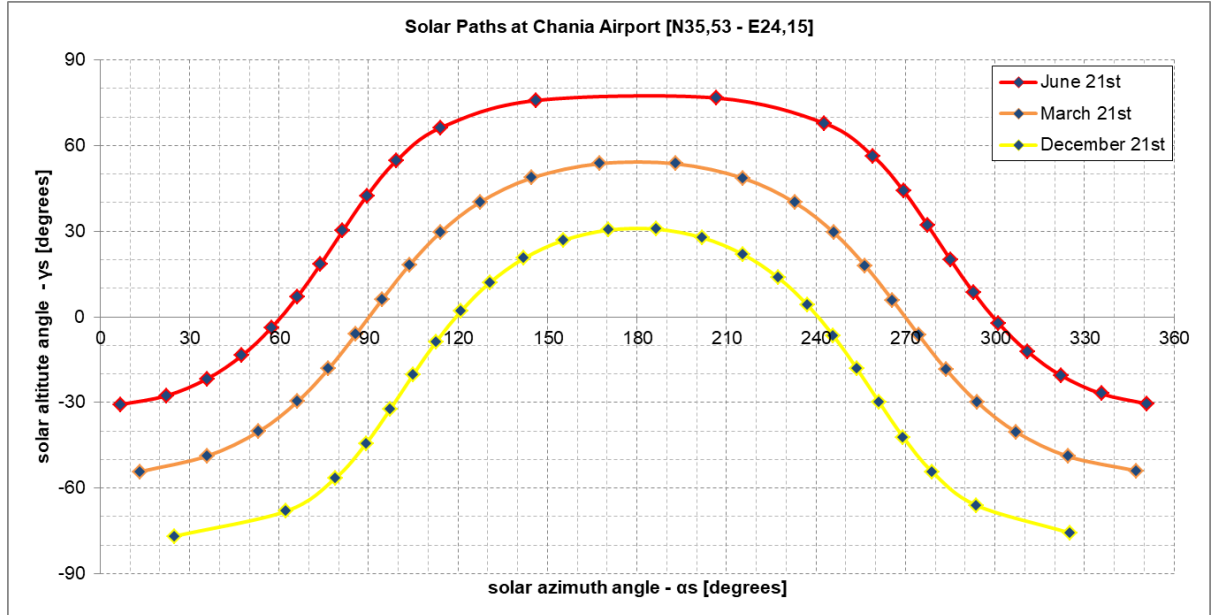

Figure A.1: Solar trajectories of an observer located at Chania Airport.

Friction velocity (u*) and Monin-Obukhov length (L) have been calculated through the Equation (A.8) and Equation (A.9), respectively.

$$u_* = \frac{k \cdot u}{\ln\left(\dfrac{z_{ref}}{z_o}\right) - \Psi_m \cdot \left(\dfrac{z_{ref}}{L}\right) + \Psi_m \cdot \left(\dfrac{z_o}{L}\right)} \tag{A.8}$$

$$L = -\frac{\rho \cdot C_p \cdot T \cdot u_*^3}{k \cdot g \cdot H} \tag{A.9}$$

where:

k : von Karman constant [0,4];

u: reference height wind speed [m/s];

The Ψ terms of the denominator of Equation (A.8) have been determined through Equations (A.10) and (A.11).

$$\Psi_m \cdot \left(\frac{z_{ref}}{L}\right) = 2 \cdot \ln\left(\frac{1+\mu}{2}\right) + \ln\left(\frac{1+\mu^2}{2}\right) - 2 \cdot \arctan(\mu) + \frac{\pi}{2} \tag{A.10}$$

$$\Psi_m \cdot \left(\frac{z_o}{L}\right) = 2 \cdot \ln\left(\frac{1+\mu_o}{2}\right) + \ln\left(\frac{1+\mu_o^2}{2}\right) - 2 \cdot \arctan(\mu_o) + \frac{\pi}{2} \tag{A.11}$$

The μ and μ_o terms in the above Equations have been calculated through Equations (A.12) and (A.13), respectively.

$$\mu = \left(1 - \frac{16 \cdot z_{ref}}{L}\right)^{\frac{1}{4}} \tag{A.12}$$

$$\mu_o = \left(1 - \frac{16 \cdot z_o}{L}\right)^{\frac{1}{4}} \tag{A.13}$$

Friction velocity and Monin-Obukhov length have been calculated iteratively by setting Ψ values to zero and determining an initial value for friction velocity. Consecutive values of L with a differentiation less than 1% have been produced after the fourth iteration.

Finally, the turbulent velocity scale w_* has been calculated through Equation (A.14).

$$w_* = \left(\frac{g \cdot H \cdot Z_{ic}}{\rho \cdot C_p \cdot T}\right)^{\frac{1}{3}} \tag{A.14}$$

A.2 Unstable Atmosphere

During stable atmospheric conditions the surface heat flux receives negative values which cause the emissions to stay near the surface, so the ground receptors measure grater values compared with the values measured during unstable atmospheric conditions. Friction velocity in stable conditions has been calculated through the Equation (A.15).

$$u_* = \frac{C_D \cdot u_{ref}}{2} \cdot \left\{ -1 + \left[1 + \left(\frac{2 \cdot u_o}{C_D^{\frac{1}{2}} \cdot u_{ref}} \right)^2 \right]^{\frac{1}{2}} \right\} \tag{A.15}$$

The above Equation includes the neutral drag coefficient (C_D) and the term u_o which have been calculated through the Equation (A.16) and (A.17), respectively.

$$C_D = \frac{k}{\ln\left(\frac{z_{ref}}{z_o} \right)} \tag{A.16}$$

$$u_o = \left(\frac{\beta_m \cdot z_{ref} \cdot g \cdot \theta_*}{T} \right)^{\frac{1}{2}} \tag{A.17}$$

where:

β_m : dimensional constant equal to 4,7;

Equation (B.17) includes the term θ_* which stands for temperature scale and it has been calculated according to Equation (A.18).

$$\theta_* = 0,09 \cdot \left(1 - 0,5 \cdot n^2 \right) \tag{A.18}$$

Since Equation (B.15) produces real solutions only for wind speeds greater than or equal to a critical value u_{cr}, this value had to be calculated through Equation (A.19).

$$u_{cr} = \left(\frac{4 \cdot \beta_m \cdot g \cdot \theta_*}{T_{ref} \cdot C_D} \right)^{\frac{1}{2}} \tag{A.19}$$

When wind speeds have been lower than u_{cr}, u_* and θ_* have been calculated through Equations (A.20) and (A.21), respectively.

$$u_* = u_* \cdot \frac{u}{u_{cr}} \tag{A.20}$$

$$\theta_* = \theta_* \cdot \frac{u}{u_{cr}} \tag{A.21}$$

With a known value of u_*, surface heat flux has been calculated through the Equation (A.22).

$$H = -\rho \cdot C_p \cdot u_* \cdot \theta_* \tag{A.22}$$

Finally, mechanical mixing height (Z_{im}) has been calculated according to the Equation (A.23).

$$Z_{im} = 2300 \cdot u_*^{\frac{3}{2}} \tag{A.23}$$

Appendix B - Methodology for the Calculation of Solar Elevation Angle (γ_s)

The methodology of this section is described thoroughly in [45]. Solar elevation angle (γ_s) is the angular elevation of the center of the solar disk above the horizontal plane. This elevation depends on the seasonal variation which is attributed to the different declination of Earth's axis towards the sun beams during the year. Solar azimuth angle (a_s) is the horizontal angle between the vertical plane containing the center of the solar disk and the vertical plane in a North-South direction. For the calculations of these angles several parameters are involved. The declination of Earth's axis is given by Equation (B.1).

$$\delta = \arcsin\left\{0,3978 \cdot \sin\left[J'-1,4+0,0355 \cdot \sin\left(J'-0,0489\right)\right]\right\} \tag{B.1}$$

where:
δ : declination [degrees];
J' : day angle [radians];

For the calculations of γs and αs, time is expressed as hour angle ω in degrees, and it is calculated trough Equation (B.2).

$$\omega = 15 \cdot \left(t-12\right) \tag{B.2}$$

where:
t : solar time [hours];

With known values of δ and ω, γ_s and α_s are calculated through Equation (B.3) and Equation (A.4), respectively given that φ Is the latitude of the studied location.

$$\gamma_s = \arcsin\left(\sin\varphi \cdot \sin\delta + \cos\varphi \cdot \cos\delta \cdot \cos\omega\right) \tag{B.3}$$

$$\alpha_s = \begin{cases} -\arccos\alpha_s, \sin\alpha_s < 0 \\ +\arccos\alpha_s, \sin\alpha_s > 0 \end{cases} \tag{B.4}$$

The conditions for the Equation (A.4) are described by Equations (B.4a) and (B.4b).

$$\cos\alpha_s = \frac{\left(\sin\varphi \cdot \sin\gamma_s - \sin\delta\right)}{\cos\varphi \cdot \cos\gamma_s} \tag{B.4a}$$

$$\sin\alpha_s = \frac{\cos\delta \cdot \sin\omega}{\cos\gamma_s} \tag{B.4b}$$

References

[1] M. Masiol and R. M. Harrison, "Aircraft engine exhaust emissions and other airport-related contributions to ambient air pollution: A review," Atmospheric Environment, vol. 95, pp. 409-455, 2014.

[2] World Health Organization. Air Quality Guidelines for Europe, 2nd ed., 2000.

[3] Directive 2008/50/EC of the European Parliament and of the Council of 21 May 2008 on Ambient Air Quality and Cleaner Air for Europe.

[4] R. A. Livingston, "Acid rain attack on outdoor sculpture in perspective," Atmospheric Environment, vol. 146, pp. 332-345, 2016.

[5] C. Muilwijk, P. J. C. Schrijvers, S. Wuerz, and S. Kenjeres, "Simulations of photochemical smog formation in complex urban areas," Atmospheric Environment, vol. 47, pp. 470-484, 2016.

[6] Intergovernmental Panel on Climate Change (IPCC). Aviation and the Global Atmosphere. Summary for Policymakers, 1999.

[7] F. Yina, V. Grewe, C. Frömming, and H. Yamashita, "Impact on flight trajectory characteristics when avoiding the formation of persistent contrails for transatlantic flights," Transportation Research Part D, vol. 65, pp. 466-484, 2018.

[8] Hellenic Statistical Authority. http://www.statistics.gr/en/statistics/-/publication/SME09/-. Accessed 9 Dec 2018.

[9] Green Agenda. http://greenagenda.gr/. Accessed 9 Dec 2018.

[10] HCAA, Aeronautical Information Publication Greece: AD 2-LGSA-1, 2012.

[11] Environmental Protection: Annex, 16, Vol. II, Aircraft Engine Emissions, ICAO, 2008.

[12] K. Rypdal, "Aircraft Emissions. Background paper to IPCC Good Practice Guidance and Uncertainty Management in National Greenhouse Gas Inventories," 2000.

[13]   Flightradar 24. http://www.flightradar24.com. Accessed 10 Jan 2018.

[14]   U.S. EPA. Fact Sheet for Trace Level SO_2 Monitoring Method. Version 2.1, 2004.

[15]   C. R. Ferguson and A. T. Kirkpatrick, Internal Combustion Engines: Applied Themodynamics: John Wiley & Sons Inc., 2001.

[16]   U. Platt and J. Stutz, Differential Optical Absorption Spectroscopy. Principles and Applications: Springer, 2008.

[17]   I. Ionel, D. Nicolae, F. Popescu, C. Talianu, L. Belegante, and G. Apostol, "Measuring Air Pollutants in an International Romania Airport with Point and Open Path Instuments," Romanian Journal of Physics, vol. 56, pp. 507-519, 2011.

[18]   Y. Zhu, E. Fanning, R. C. Yu, Q. Zhang, and J. R. Froines, "Aircraft emissions and local air quality impacts from takeoff activities at a large International Airport," Atmospheric Environment, vol. 45, pp. 6526-6533, 2011.

[19]   F. Shirmohammadi, M. H. Sowlat, S. Hasheminassab, A. Saffari, G. Ban-Weiss, and C. Sioutas, "Emission rates of particle number, mass and black carbon by the Los Angeles International Airport (LAX) and its impact on air quality in Los Angeles," Atmospheric Environment, vol. 151, pp. 82-93, 2017.

[20]   E. Pecorari, A. Mantovani, G. Franceschini, D. Bassanoc, L. Palmeri, and G. Rampazzo, "Analysis of the effects of meteorology on aircraft exhaust dispersion and deposition using a Lagrangian particle model," Science of the Total Environment, vol. 541, pp. 839-856, 2016.

[21]   S. L. Kuzu, "Estimation and dispersion modeling of landing and take-off (LTO) cycle emissions from Atatürk International Airport," Air Qual Atmos Health, vol. 11, pp. 153-161, 2018.

[22]   I. Simonetti, S. Maltagliati, and G. Manfrida, "Air quality impact of a middle size airport within an urban context through EDMS simulation," Transportation Research Part D, vol. 40, pp. 144-154, 2015.

[23] FAA. Emissions and Dispersion Modeling System (EDMS) User's Manual. FAA-AEE-07-01. Washington, DC, June, 2013.

[24] U.S. EPA. User's Guide for the AMS/EPA Regulatory Model (AERMOD). EPA-454/B-16-011, December, 2016.

[25] C. D. Cooper and F. C. Alley, Air Pollution Control, A Design Approach, 3rd ed., 2002.

[26] A. A. Abdel-Rahman, "On the Atmospheric Dispersion and Gaussian Plume Model," presented at the 2nd International Conference on Waste Management, Water Pollution, Air Pollution, Indoor Climate (WWAI'08), Corfu, Greece, 2008.

[27] R. Webster and M. A. Oliver, Geostatistics for Environmental Scientists, 2nd ed.: John Wiley & Sons Ltd, 2007.

[28] U.S. Geological Survey. https://earthexplorer.usgs.gov/. Accessed 15 Mar 2018.

[29] Ogimet. https://www.ogimet.com/metars.phtml.en. Accessed 4 Nov 2017.

[30] Document 9889. Airport Air Quality Manual: ICAO (2011).

[31] Air pollutant emission inventory guidebook 2016, EMEP/EEA, 2017.

[32] A. Petzold, C. Stein, S. Nyeki, M. Gysel, E. Weingartner, U. Baltensperger, et al., "Properties of jet engine combustion particles during the PartEmis experiment: Microphysics and Chemistry," Geophysical Rerearch Letters, vol. 30 (13), 1719, 2003.

[33] ICAO Engine Emissions Data Bank. https://www.easa.europa.eu/easa-and-you/environment/icao-aircraft-engine-emissions-databank. Accessed 4 Apr 2018.

[34] IPCC Guidelines for National Greenhouse Gas Inventories, 2006.

[35] U.S. EPA. User's Guide for the AERMOD Meteorological Preprocessor (AERMET). EPA-454/B-16-010. North Carolina, U.S.A., December, 2016.

[36] A. J. Cimorelli, S. G. Perry, A. Venkatram, J. C. Weil, R. J. Paine, R. B. Wilson, et al., "AERMOD: A Dispersion Model for Industrial Source Applications. Part I: General Model Formulation and Boundary Layer Characterization," Journal of Applied Meteorology, vol. 44, pp. 682-693, 2005.

[37] L. T. Carbonell, J. R. Oliva, L. C. Garea, M. S. Gácita, E. M. Ruiz, and N. D. Rivero, Environmental Impact Assessments: Method for the Estimation of the Convective Mixing Height Aimed to Atmospheric Local Dispersion Modeling: Nova Science Publishers Inc., 2009.

[38] T. C. Lieuwen and V. Yang, Gas Turbine Emissions: Cambridge University Press, 2013.

[39] S. R. H. Barrett, R. E. Britter, and I. A. Waitz, "Impact of aircraft plume dynamics on airport local air quality," Atmospheric Environment, vol. 74, pp. 247-258, 2013.

[40] J. S. Kinsey, Y. Dong, D. C. Williams, and R. Logan, "Physical characterization of the fine particle emissions from commercial aircraft engines during the Aircraft Particle Emissions eXperiment (APEX) 1-3," Atmospheric Environment, vol. 44, pp. 2147-2156, 2010.

[41] C. Psanis, E. Triantafyllou, M. Giamarelou, M. Manousakas, K. Eleftheriadis, and G. Biskos, "Particulate matter pollution from aviation-related activity at a small airport of the Aegean Sea Insular Region," Science of the Total Environment, vol. 596–597, pp. 187-193, 2017.

[42] T. Boden and B. Andres. Carbon Dioxide Information Analysis Center. http://cdiac.ess-dive.lbl.gov/trends/emis/top2014.tot . Accessed 4 Oct 2018.

[43] Marine Traffic. https://www.marinetraffic.com/. Accessed 18 Nov 2018.

[44] E. Batchvarova and S. E. Gryning, "Applied model for the growth of the daytime mixed layer," Boundary Layer Meteorology, vol. 56, pp. 261-274, 1991.

[45] T. Markvart and L. Castaner, Practical Handbook of Photovoltaics: Fundamentals and Applications: Elsevier.